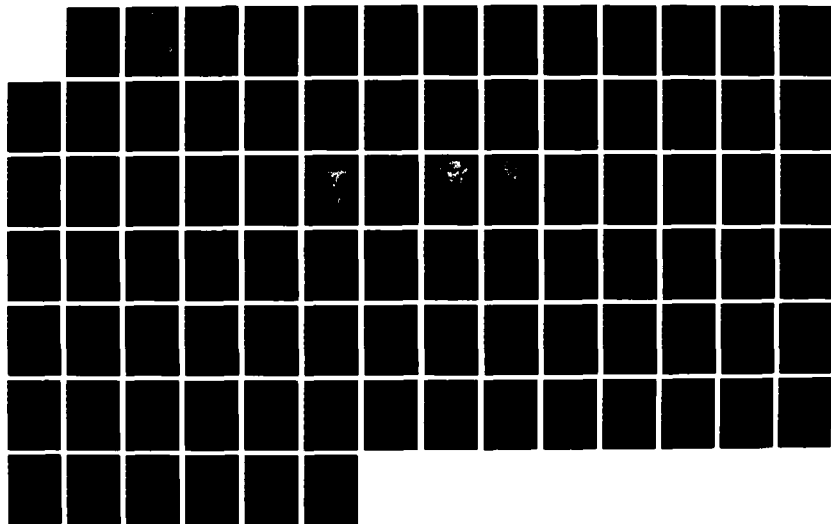OBSERVATION OF GRAVITY WAVES DURING THE GENESIS OF
ATLANTIC LOWS EXPERIMENT(U) AIR FORCE INST OF TECH
WRIGHT-PATTERSON AFB OH D M WOJTAK AFIT/CI/NR-87-48T
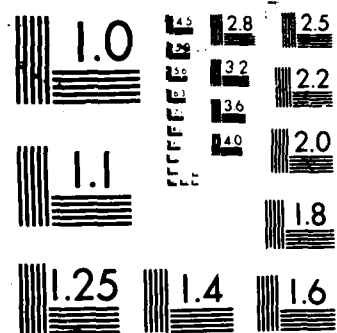
OBSERVATION OF GRAVITY WAVES
DURING THE
GENESIS OF ATLANTIC LOWS EXPERIMENT

by

Donna M. Wojtak

A thesis submitted to the Graduate Faculty of
North Carolina State University
in partial fulfillment of the
requirements for the Degree of
Master of Science

Department of Marine, Earth and Atmospheric Sciences

Raleigh

1987

Approved by:

G. Watson

P. Bloomfield

M. DeMaria -- Chairman

87 10 14 254

REPORT DOCUMENTATION PAGE		READ INSTRUCTIONS BEFORE COMPLETING FORM
1. REPORT NUMBER AFIT/CI/NR 87-48T	2. GOVT ACCESSION NO. AD A186819	3. RECIPIENT'S CATALOG NUMBER
4. TITLE *(and Subtitle)* Observation of Gravity Waves During The Genesis Of Atlantic Lows Experiment		5. TYPE OF REPORT & PERIOD COVERED THESIS/DISSERTATION
		6. PERFORMING ORG. REPORT NUMBER
7. AUTHOR(s) Donna M. Wojtak		8. CONTRACT OR GRANT NUMBER(s)
9. PERFORMING ORGANIZATION NAME AND ADDRESS AFIT STUDENT AT: North Carolina State University		10. PROGRAM ELEMENT, PROJECT, TASK AREA & WORK UNIT NUMBERS
11. CONTROLLING OFFICE NAME AND ADDRESS AFIT/NR WPAFB OH 45433-6583		12. REPORT DATE 1987
		13. NUMBER OF PAGES 75
14. MONITORING AGENCY NAME & ADDRESS(*if different from Controlling Office*)		15. SECURITY CLASS. *(of this report)* UNCLASSIFIED
		15a. DECLASSIFICATION DOWNGRADING SCHEDULE

16. DISTRIBUTION STATEMENT *(of this Report)*

APPROVED FOR PUBLIC RELEASE; DISTRIBUTION UNLIMITED

17. DISTRIBUTION STATEMENT *(of the abstract entered in Block 20, if different from Report)*

18. SUPPLEMENTARY NOTES
APPROVED FOR PUBLIC RELEASE: IAW AFR 190-1

LYNN E. WOLAVER 17 Aug 87
Dean for Research and
Professional Development
AFIT/NR

19. KEY WORDS *(Continue on reverse side if necessary and identify by block number)*

20. ABSTRACT *(Continue on reverse side if necessary and identify by block number)*
ATTACHED

DD ₁ FORM ₇₃ 1473   EDITION OF 1 NOV 65 IS OBSOLETE

87   10   13   254

ABSTRACT

WOJTAK, DONNA, M. Observation of Gravity Waves during the Genesis of Atlantic Lows Experiment. (Under the direction of Mark DeMaria.)

This research was initiated as a direct result of the Genesis of Atlantic Lows Experiment (GALE) which was conducted from 15 January to 15 March 1986. The principle objective of GALE was to study various mesoscale processes and their role in cyclogenesis along the East Coast of the United States. A supporting objective was to study the role of gravity waves in the organization of precipitation bands.

The three-day period from 4 to 6 February was chosen for this study since several mesoscale disturbances resembling gravity waves passed through the data network. A high-pass spectral filter was applied to the pressure, temperature, and wind fields to remove the diurnal and semi-diurnal trends. In this way, the higher frequencies with periods of 8 hours or less could be isolated. The filtered data were plotted using an objective analysis scheme which interpolated the data to an evenly spaced grid. A spatial filter was also applied to remove wavelengths less than twice the original station spacing. The horizontal divergence was calculated using the filtered wind field.

Four gravity wave cases were identified from the surface pressure and divergence fields. Phase speeds ranged from 20-40 m s^{-1} with wavelengths from 200-400 km, and

amplitudes of 0.25-2.0 mb. Precipitation was usually not associated with the waves. The last case on 6 February, which was the one most well-defined, did have a precipitation pattern which followed its movement.

Further analysis was performed on each case using sounding data. A comparison with linear gravity wave theory suggests that the gravity waves were freely propagating rather than a surface response to upper level forcing. While the waves were not directly associated with a frontal system, the Appalachian Mountains may have played a role in their formation.

BIOGRAPHY

Donna M. Wojtak was born in Brooklyn, New York, on September 10, 1953. She graduated from Tappan Zee High School, Orangeburg, New York, in 1971.

She attended the State University College of New York at Brockport, New York from September 1971 to May 1973. In September 1973, she entered St. Thomas Aquinas College, Sparkill, New York and received a Bachelor of Science degree with honors in Mathematics during May 1975.

In July 1976, the author was commissioned a Second Lieutenant in the United States Air Force. She has been assigned to the following locations since entering the Air Force:

Texas A&M University	July 1976 - August 1977
Offutt AFB, Omaha NE	August 1977 - June 1979
Shemya AFB, Alaska	June 1979 - June 1980
Langley AFB, Hampton VA	June 1980 - October 1982
Shaw AFB, Sumter SC	October 1982 - August 1985

While stationed at Shaw AFB, the author earned a Master of Science degree in Human Resources Management from Golden Gate University. In August 1985, she entered the Graduate School at North Carolina State University to begin studies toward a Master of Science degree in Meteorology.

ACKNOWLEDGEMENTS

TABLE OF CONTENTS

LIST OF TABLES

LIST OF FIGURES

1. INTRODUCTION

A linear analysis of the set of equations which describe motions in the atmosphere reveals five wave solutions. Two solutions describe sound waves and a third, Rossby or planetary waves. The final two solutions detail the motion resulting from gravity waves. It is the occurrence of gravity waves in the atmosphere which is the subject of this research study.

Simply put, a gravity wave occurs in a stably stratified atmosphere when a parcel of air undergoes buoyancy oscillations about its equilibrium state (Holton, 1979). For this reason, gravity waves have often been called buoyancy waves. But gravity waves are a complex phenomenon which, when in the form of a mountain wave, can cause severe clear-air turbulence (Hooke and Hardy, 1975). When associated with cyclogenesis, gravity waves can augment the occurrence of precipitation (Gedzelman and Rilling, 1978).

There have been many observations of gravity waves in the atmosphere. Bosart and Cussen (1973) observed extensive gravity wave activity in the southeastern United States within the cold air north of a quasi-stationary front during the period from 3 to 5 December 1968. The gravity wave they studied had a 3.5 mb amplitude, a propagation speed of 10 - 15 m s^{-1} and a life cycle of

approximately 15 hours. Precipitation occurred to the east of the eastward moving wave and ended after wave passage. Bosart and Cussen concluded that thunderstorm activity was the initial triggering mechanism.

Gossard and Munk (1954) observed gravity wave oscillations during seven days from April 1952 to May 1953 at La Jolla, California. These oscillations had periods from 5 to 15 minutes, phase speeds of approximately 10 m s^{-1} and wavelengths from 4 to 10 km. Gossard and Munk found that the oscillations occurred in conjunction with large temperature inversions over the area and were often accompanied by fog or very low stratus. These conditions occur in southern California when the area is under the influence of a well-developed Pacific high pressure system.

Cunning (1974) observed gravity waves during a two week period in October 1971 in the Miami, Florida area. Amplitudes ranged from 0.4 mb to 1.0 mb and phase speeds were approximately 30 m s^{-1}. Cunning found that within southern Florida, waves occur almost continuously regardless of time of day or year.

In these and other case studies (e.g., Bosart, 1973; Donn et al., 1973; Herron et al., 1969) it has been shown that gravity waves are observed with a wide range of wavelengths, amplitudes, and phase speeds. The one limiting factor in these studies is that data were available from just a few stations.

Data used in this study of gravity waves were obtained
during the Genesis of Atlantic Lows Experiment (GALE)
(Hobbs et al., 1985). This multi-university, multi-agency
field experiment encompassed a two-month time period from
15 January to 15 March 1986. GALE had several objectives.
These were to: 1) describe the airflow, mass, and moisture
fields in East Coast winter storms with emphasis on mesos-
cale processes; 2) understand physical mechanisms control-
ling the formation and rapid development of East Coast
storms; and 3) develop and test numerical models for the
prediction of East Coast storms. A supporting objective
was to study the role of gravity waves as a mechanism in
the development of precipitation bands.

GALE provided an excellent medium to observe gravity
waves. The annual cycle of wave amplitudes in mid-
latitudes snows a peak from October through March
(Gedzelman, 1983). GALE took place during the latter part
of tnis time period. In addition, large amounts of data
were available for the entire two-month period. A network
of fifty Portable Automated Mesonet (PAM II) stations
extending from South Carolina to Virginia provided, among
otner variables, pressure, temperature, wind speed and
direction, and rainfall data every 5 minutes. The PAM II
stations were approximately 60 km apart, providing a high
resolution data field.

Because of the vast amount of data available, the

3

three-day period from 4 to 6 February was chosen for this research. This particular time frame was selected because several mesoscale disturbances resembling gravity waves passed through the data network. To isolate and analyze these gravity waves, a high-pass spectral filter is applied to the pressure, temperature, and wind fields. This removes both the diurnal and semi-diurnal trends to isolate the higher frequency oscillations with periods of 8 hours or less. The filtered data are interpolated to an evenly spaced grid using an objective analysis scheme (Barnes, 1964, 1973). A spatial filter is also applied (Shapiro, 1975) to remove wavelengths less than twice the original station spacing. The horizontal divergence field is calculated from the filtered wind field using centered finite differences.

From the analysis of the surface pressure perturbation field and the horizontal divergence, four gravity wave cases are identified. Phase speeds and wavelengths are calculated directly from the plotted data. To further study the four cases, sounding data are used to compare the observed characteristics of the waves with linear gravity wave theory. Synoptic data are also studied to determine possible origins of the waves.

4

2. CURRENT THEORY

Gravity waves are thought to be prevalent throughout the atmosphere. Atkinson (1981) states that gravity waves can occur from the surface to heights above 20 km. Other wave characteristics are also quite variable. Wavelengths can range from 5 to 500 km, phase speeds from 10 to 50 m s^{-1} and periods from minutes to hours.

Wave occurrence is often associated with vertical stability and wind shear (Atkinson, 1981; Gedzelman and Rilling, 1978). Both vertical stability and wind shear are reflected in a calculation of the Richardson number (Ri) given by:

$$Ri = \frac{\frac{g}{\theta} \frac{\partial \theta}{\partial z}}{\left(\frac{\partial U}{\partial z}\right)^2} \qquad (2.1)$$

where g is the acceleration of gravity, θ the potential temperature, U the horizontal wind speed and z is height. Atkinson (1981) indicates that waves occur in layers where the Richardson number is less than 0.50. Gedzelman and Rilling (1978) related minimum Richardson number to wave amplitudes (Figure 2.1). They indicate that the critical Richardson number for large-amplitude waves is 0.25. Gedzelman and Rilling also found that the waves tend to move with the wind speed and direction at the level of

5

FORBIDDEN REGION
FOR AMPLITUDES
OF SHEAR GENERATED
GRAVITY WAVES

wave amplitude (μbar)

(largest waves, 6hr. average)
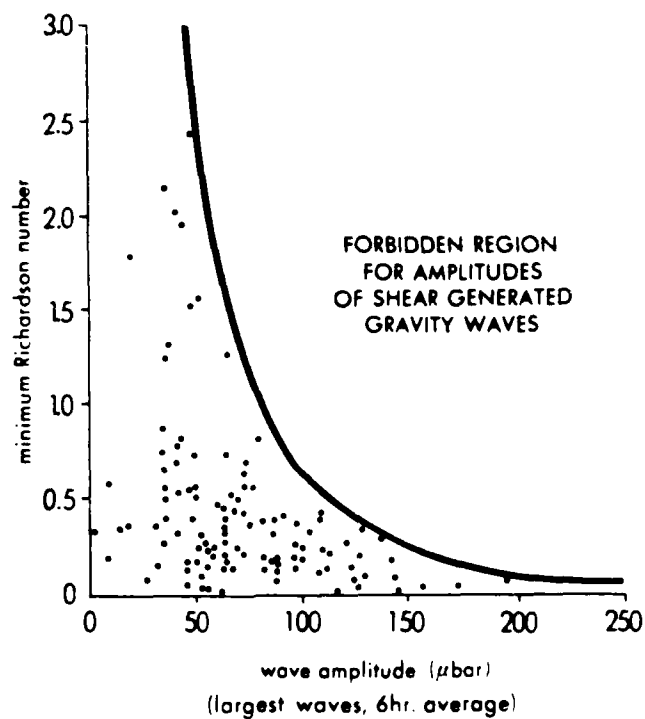
Figure 2.1 Wave amplitudes as a function of minimum Richardson number in the sounding. The envelope indicates tnat large-amplitude waves are not expected from shear instability when Ri_{min} exceeds 0.25 (after Gedzelman and Rilling, 1978).

6

minimum Richardson number in the sounding.

In a stably stratified atmosphere, gravity waves can propagate without vertical wind shear. The simplest system of equations which includes this effect are the vertically averaged equations of motion for a hydrostatic fluid (Bannon, 1979). These equations can be written as:

$$\frac{du}{dt} - fv = -g'\frac{\partial h}{\partial x} \qquad (2.2)$$

$$\frac{dv}{dt} + fu = -g'\frac{\partial h}{\partial y} \qquad (2.3)$$

$$\frac{dh}{dt} + h\left(\frac{\partial u}{\partial x} + \frac{\partial v}{\partial y}\right) = 0 \qquad (2.4)$$

where $\qquad g' = g(1 - \theta_1/\theta_2),$ $\qquad (2.5)$

and $\qquad \dfrac{d}{dt} = \dfrac{\partial}{\partial t} + u\dfrac{\partial}{\partial x} + v\dfrac{\partial}{\partial y} \cdot \qquad (2.6)$

In Equations 2.2 through 2.4, f is the Coriolis parameter and h is the fluid depth. The above equations assume that the potential temperature (θ_1) is constant in a layer of depth h with a potential temperature θ_2 above this layer. Assuming one-dimensional ($\partial/\partial y = 0$), non-rotating flow (f = 0), a linear analysis of Equations 2.2 to 2.4 using the perturbation method (Holton, 1979), results in the equation for the phase speed, c, given by:

$$c = \bar{u} \pm \{ gH [1 - (\theta_1/\theta_2)]\}^{1/2} \qquad (2.7)$$

7

wnere $\bar{u}$ is the wind speed in the layer and H is the mean depth of the layer.

A determination of whether a gravity wave is forced by vertical wind shear or is freely propagating can help determine the origin of the wave. For instance, studies have been done relating the jet stream and gravity waves (Donn et al., 1973; Herron and Tolstoy, 1969; Tolstoy and Herron, 1969; Mastrantonio et al., 1976). Topographic features, convective activity, and frontal systems are also possible mechanisms in the formation of gravity waves in the atmosphere.

3. DATA ANALYSIS TECHNIQUES

3.1 Portable Automated Mesonet System Data

Data used in this research study were obtained from tne Portable Automated Mesonet (PAM II) System deployed during GALE (Figure 3.1). These stations extended from South Carolina to Virginia and were approximately 60 km apart. The PAM II stations provided fifteen different data values every 5 minutes. The six parameters chosen for this study included pressure (mb), temperature ($^{\circ}$C), dewpoint temperature ($^{\circ}$C), rainfall amount (mm) and the u and v components of the wind (m s^{-1}). For the purpose of this research, data at 10-minute intervals were used during the three-day observation period versus the 5-minute data available. The primary reason for this was limited computer disk storage space. By comparing plots of the 5-and-10 minute data, it was determined that the features of interest could be resolved witn the 10-minute data.

3.2 Preliminary Data Processing

3.2.1 Data Correction

For tne three-day period, each day was processed as a separate data set. If a station had a data value missing two or more times in a row, the station was not included in calculations involving the particular parameter. If a single value was missing, a replacement value was

9
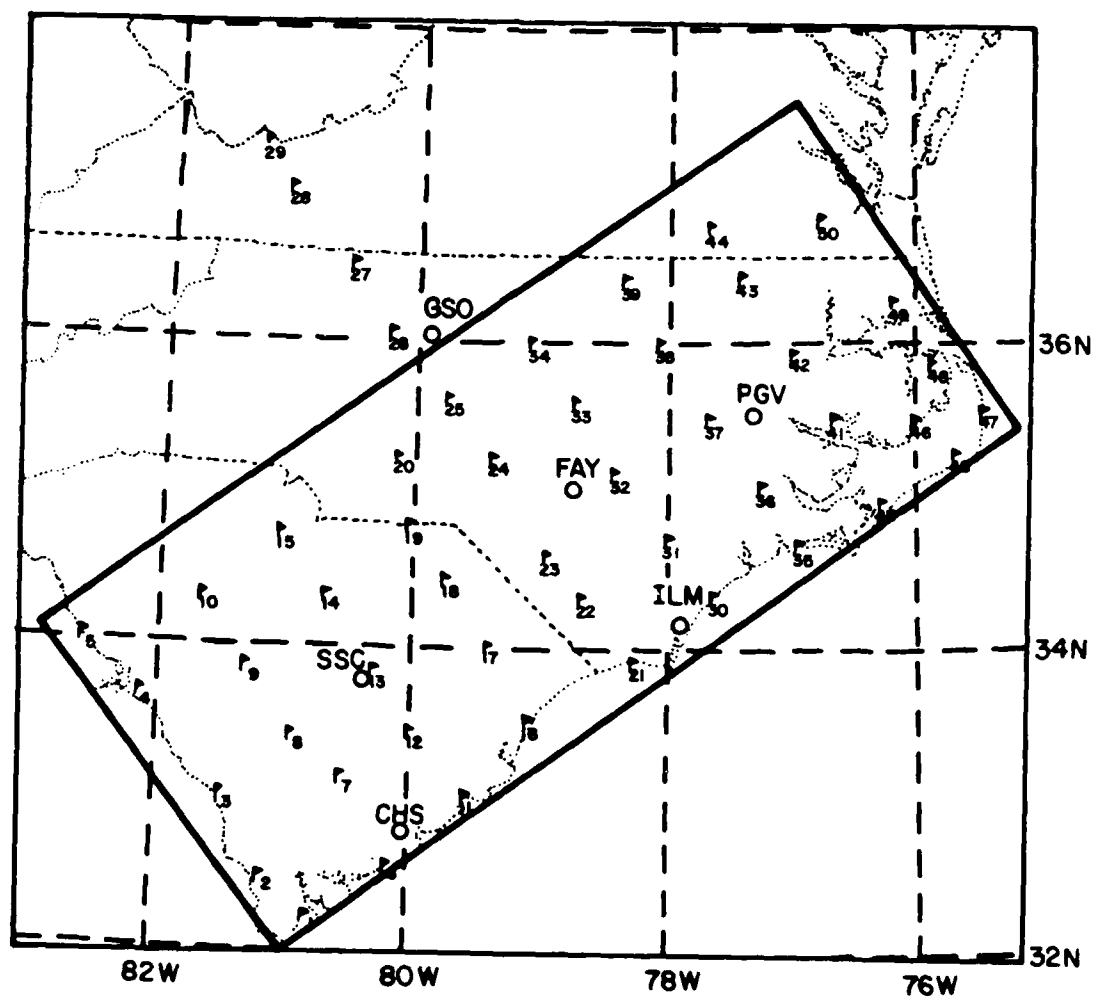
Figure 3.1 The 50 station PAM II network. Rectangular box encompasses Barnes analyzed grid. Sounding stations are indicated by a small circle and three letter identifier.

10

calculated by taking an average of the data value prior to and following the missing one. For the endpoints of the data set, a missing value was replaced by the preceding or following value as appropriate. A station was also eliminated from further processing if it contained obviously erroneous data values. For any one day or data parameter, five stations or less were eliminated.

3.2.2 Fourier Transform

In order to isolate the high frequency oscillations, the data from each station were Fourier transformed in time. Before applying the transform, the linear trend during a 24-hour period was removed from each station. A calculation was made of the slope (b) and y-intercept (a) of the least squares line. The residuals were calculated by subtracting the value given by a + bt from the data values. The Fourier transform was then applied as follows:

$$\hat{P}_n = 1/M \sum_{j=0}^{M-1} P_j \, e^{(-2\pi i n j)/M} \tag{3.1}$$

where M is the total number of data points, and P_j is a residual (detrended data point). The value of n in Equation 3.1 goes from 0 to M-1. The above transform is fairly standard and details can be found in most time series texts (e.g., Bloomfield, 1976).

The squared amplitudes were averaged over all the

11

stations by frequency. Figure 3.2 is the average of the squared amplitude versus frequency plotted by day for pressure. The periods in hours corresponding to each frequency and the amplitudes in mb are also shown on the diagram. Since the P_j are real, only half of the frequencies need to be plotted. The amplitudes corresponding to the frequencies greater than the ones represented in Figure 3.2 and up to M = 144 are just a mirror image of those plotted.

The significance of the average of the squared amplitude versus frequency plots is in identifying peaks along the general trend in order to isolate frequencies of interest. For instance, if a peak occurs at x = 24, as it does in Figure 3.2a, a wave with a period of one hour occurred with a higher amplitude than the general trend which is decreasing with higher frequencies. For this research, it was decided that frequencies with periods of 8 hours or less needed to be isolated. In other words, the diurnal and semi-diurnal trends would be eliminated.

3.2.3 High-Pass Filter

In order to remove the diurnal and semi-diurnal trends in the data, a high-pass filter was performed. This involved setting the real and imaginary parts of amplitudes with a frequency of 1 or 2 equal to zero. An inverse transform is then performed using:
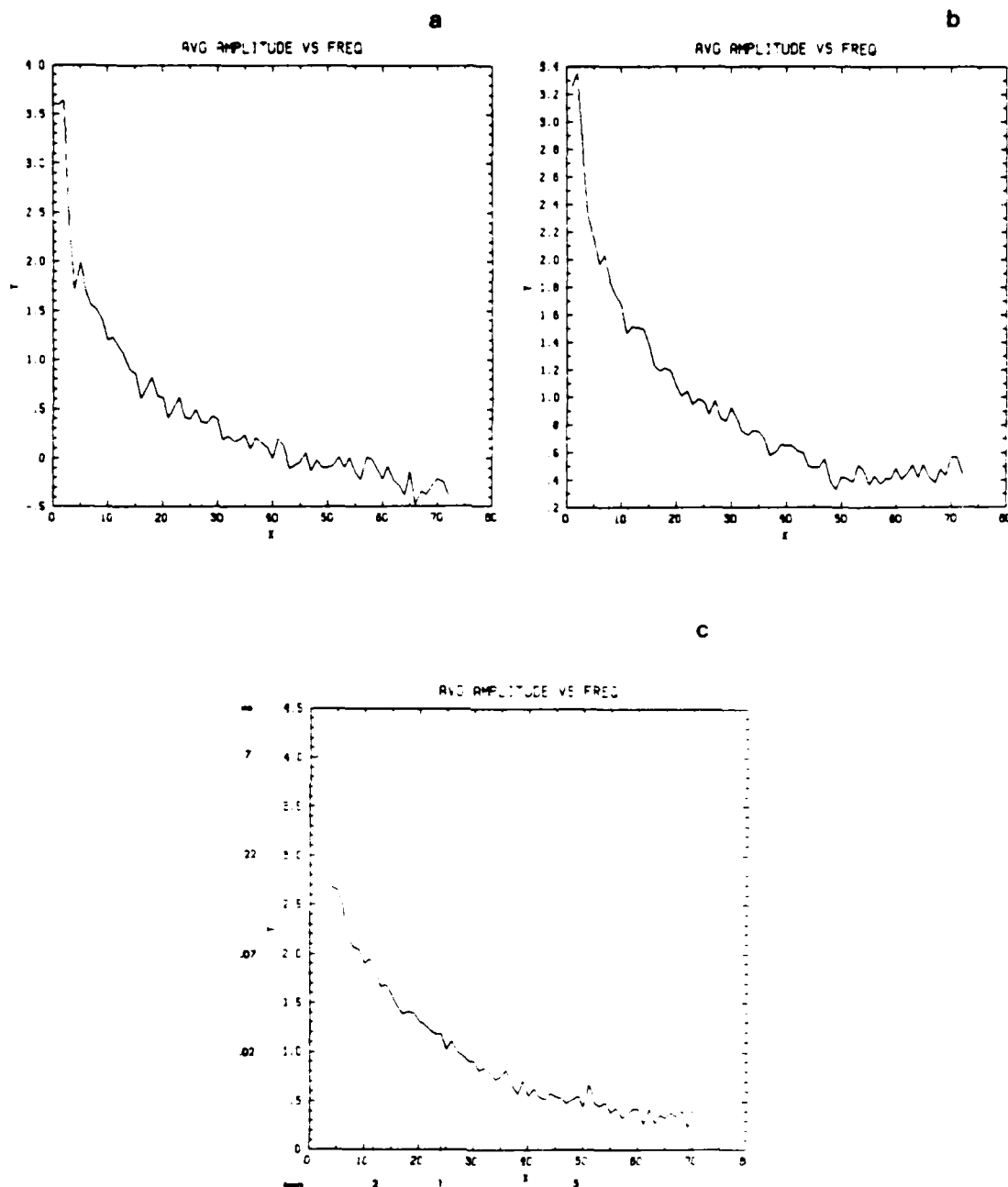
Figure 3.2 Average of the squared amplitude (y) versus frequency (x) for (a) 4 February 1986; (b) 5 February 1986; (c) 6 February 1986. (Pressure). Periods in hours and amplitudes in mb shown in (c) also apply for the other two days.

$$P_j = \sum_{n=0}^{M-1} \hat{P}_n \, e^{(2\pi inj)/M} \qquad (3.2)$$

where parameters are the same as for Equation 3.1.

Figure 3.3 represents a pressure versus time plot before the data have been filtered. When the diurnal and semi-diurnal trends are removed by the above procedures, the resulting perturbation pressure versus time plot is shown in Figure 3.4.

3.3 Barnes Analysis

An objective analysis (Barnes, 1964, 1973) was applied to the filtered data to interpolate the data to an evenly spaced grid. The area encompassing the grid is shown in Figure 3.1. There are 33 grid points in the x-direction and 15 in the y-direction. Spacing between grid points is 20 km.

The Barnes scheme calculates a grid point value using a distance weighted average of the surrounding station values. The scheme uses all stations within a specified radius of influence. The radius of influence used here is 130 km. This influence radius was chosen so that at least 3 stations would be included in the calculation of each grid point value. For the entire grid network, an average of 8 stations was used per grid point. The weight function (WT) is given by:

14
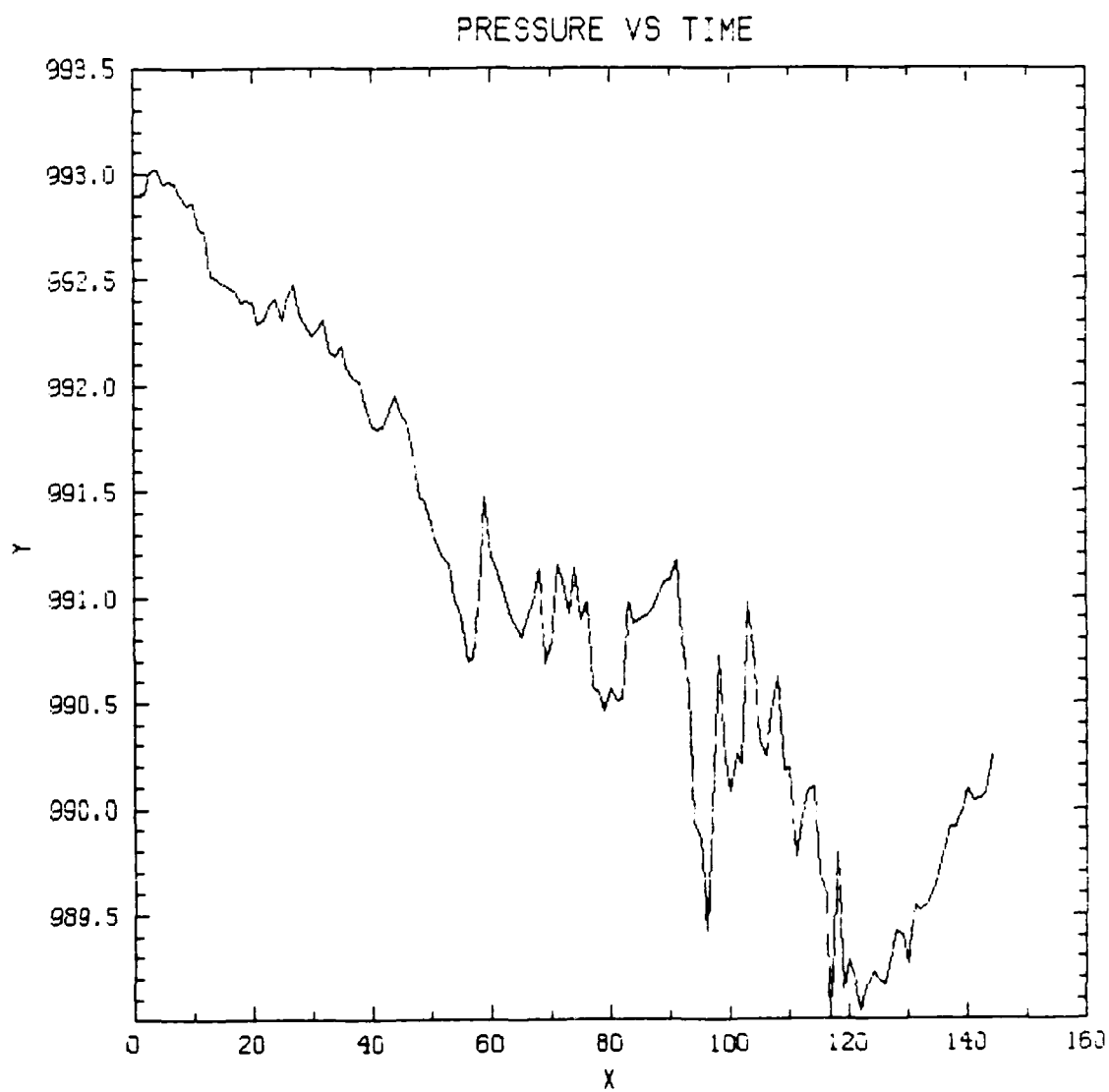
PRESSURE VS TIME

Figure 3.3 Unfiltered pressure in millibars (y) versus time (x) for station 15 on 5 February 1986. Time is in 10-minute intervals.

15
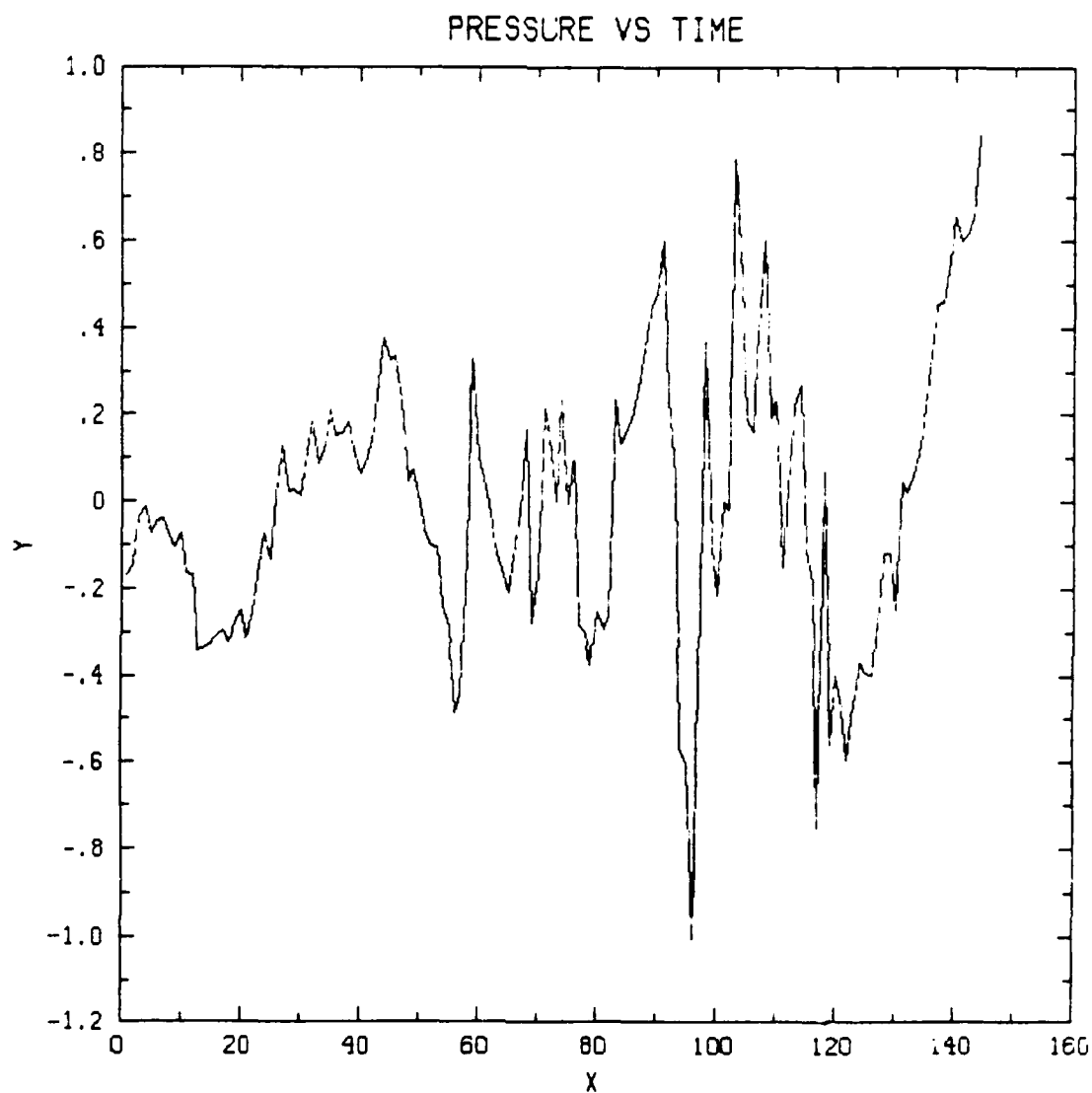
Figure 3.4 Perturbation pressure in millibars (y) versus
time (x) for station 15 on 5 February 1986. Diurnal and
semi-diurnal trend removed. Time is in 10-minute
intervals.

16

$$WT \ = \ \exp(-RAD^2/RE^2) \qquad (3.3)$$

where RAD is the distance from a station to the grid point and RE is a specified e-folding radius. If the e-folding radius is not chosen correctly, too much or too little smoothing of the data field will occur. The e-folding radius of the weight function used in this study is 50 km. Various values were tested and 50 km provided optimum results.

After the analysis described above is applied, two additional iterations of the Barnes analysis are performed to regain some details smoothed by the first pass of the scheme. This is done by linearly interpolating the gridded values back to the station locations. The interpolated station values are subtracted from the original station values and the objective analysis is performed on these differences. The gridded differences are then added to the grid values calculated as the first-guess. Doing two iterations of the differences gave grid values with a reasonable amount of smoothing.

3.4 Spatial Filter

An additional spatial filter (Shapiro, 1975) was applied to the grid values as a last step in the processing routine. This was done in order to eliminate wavelengths less than twice the original station spacing, which cannot

17

be resolved. If $A_{i,j}$ represents a grid value, the first step in the spatial filter is to calculate:

$$B_{i,j} = 0.25A_{i+1,j} + 0.5A_{i,j} + 0.25 A_{i-1,j} \qquad (3.4)$$

where $B_{i,j}$ is a new grid value. The second step is calculated by:

$$C_{i,j} = 0.25B_{i,j+1} + 0.5B_{i,j} + 0.25B_{i,j-1} \qquad (3.5)$$

where $C_{i,j}$ is a new and final grid value. Equation 3.4 is a smoothing in the x-direction and Equation 3.5 is a smoothing in the y-direction. In the case of the spatial filter, two iterations were performed.

4. SYNOPTIC SITUATION

Figures 4.1 through 4.3 show the surface weather, 500-millibar height contours, highest and lowest temperatures, and precipitation areas and amounts for 4-6 February 1986, respectively. The surface and 500 mb maps are valid at 7:00 a.m. EST (12 GMT). Shading indicates precipitation. The 500-millibar height contours are labeled in dekameters above sea level. Isotherms ($^\circ$C) are shown as dashed lines. The highest and lowest temperature chart shows the maximum temperature for the 12-hour period ending at 7:00 p.m. EST (00 GMT) of the previous day and the minimum temperature for the 12-hour period ending 7:00 a.m., EST (12 GMT). The shaded areas on the precipitation area and amounts chart indicate precipitation during the 24 hours ending at 7:00 a.m., EST (12 GMT) with amounts to the nearest hundredth of an inch. Incomplete totals are underlined and a "T" represents a trace of precipitation. Snow depth on the ground in inches are indicated by dashed lines and is valid at 7:00 a.m., EST (12 GMT).

On 4 February 1986 (Figure 4.1), there was a surface low pressure center in the Kansas-Missouri area with a cold front extending through the eastern half of Texas and a warm front extending eastward into the Carolinas. Surface winds were light in the GALE area and precipitation occurred to the north of the area as indicated by both the

19
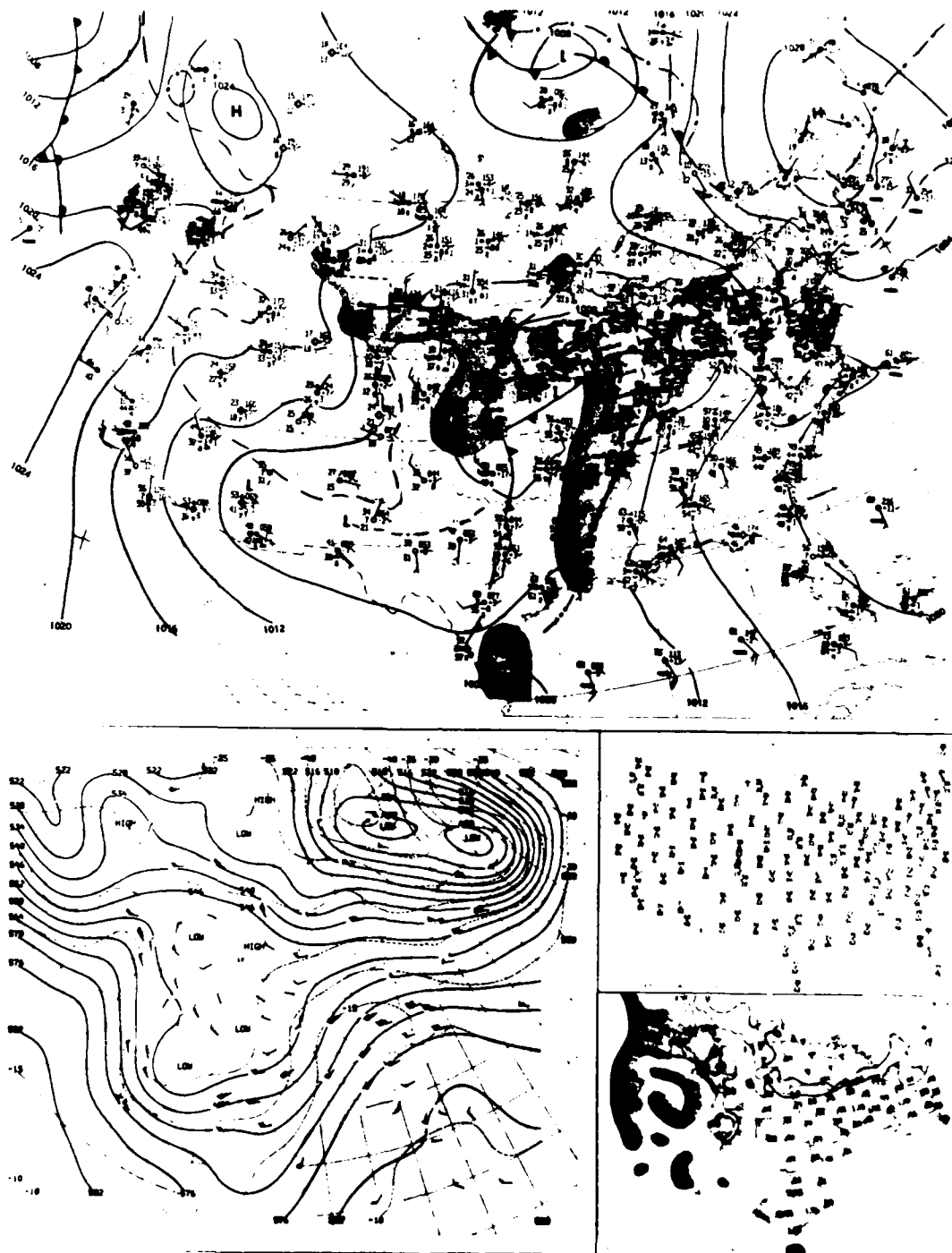
Figure 4.1 Surface weather, 500-millibar contours, Highest
and Lowest Temperature, and Precipitation Areas and Amounts
for 7:00 am, EST, 4 February 1986. See text for details.

20

surface weather map and the precipitation areas and amounts
chart. The six-hourly position of the surface front in the
GALE area on 4 February is shown in Figure 4.4a. On the
500-millibar height contour chart (Figure 4.1), the long
wave trough is to the west of the GALE area with winds in
the GALE area averaging 45-50 knots from the west.

On 5 February 1986 (Figure 4.2), the low has tracked
to the northeastern United States. The front in the GALE
area has moved north as is also indicated by Figure 4.4b.
Surface winds continue to be light in the GALE area and
precipitation is indicated. On the 500-millibar height
contour chart (Figure 4.2) the winds in the GALE area are
now from the southwest and have increased to 50-75 knots.

By 6 February 1986 (Figures 4.3 and 4.4c), a front is
again moving into the GALE area. There is a surface low in
Arkansas well to the west of the GALE area associated with
this front. Surface winds remain light and there is exten-
sive precipitation all along the East Coast. At 500-
millibars the winds speed in the GALE area have decreased
to 35-45 knots.
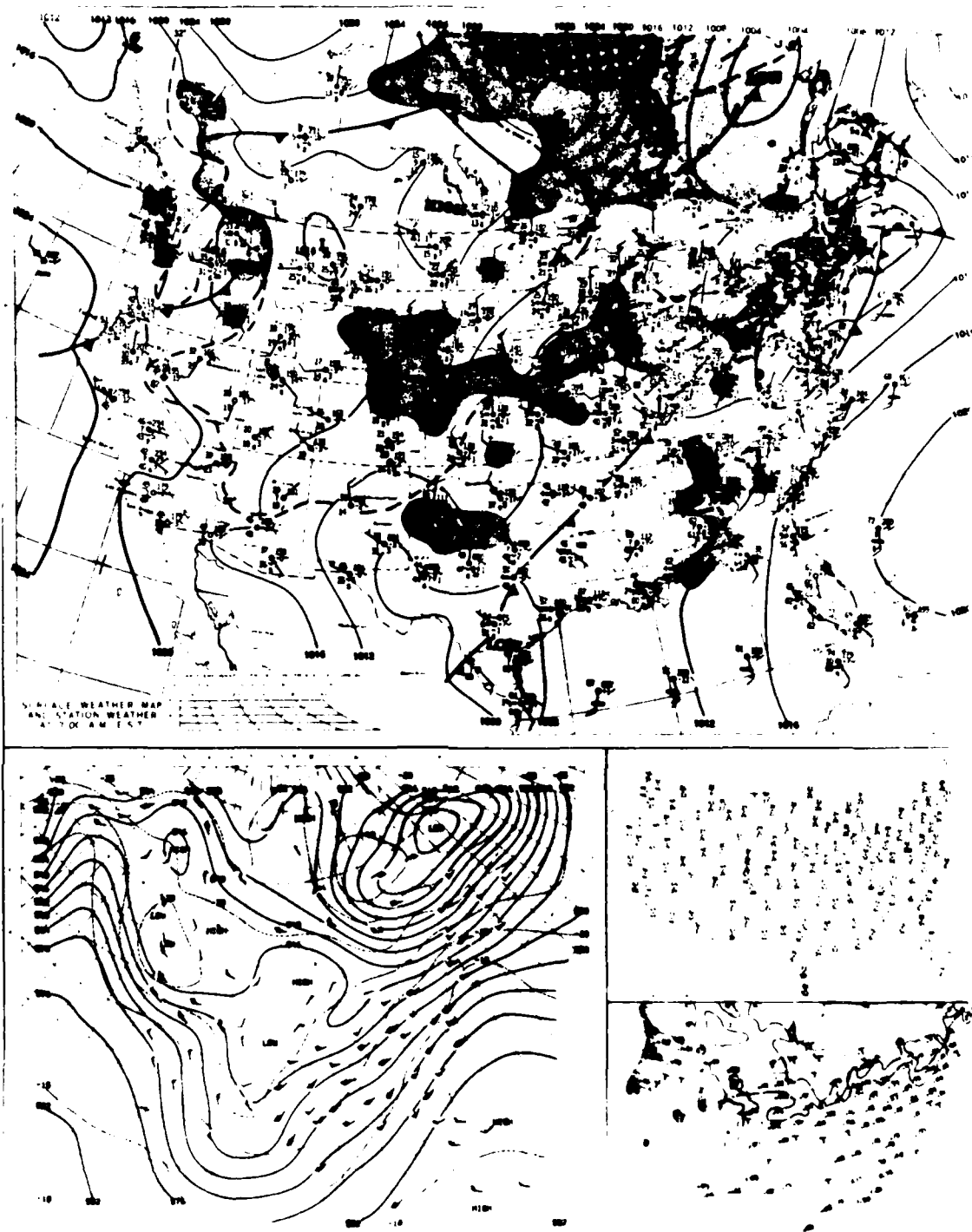
Figure 4.2 Same as Figure 4.1, except for 5 February 1986.

22
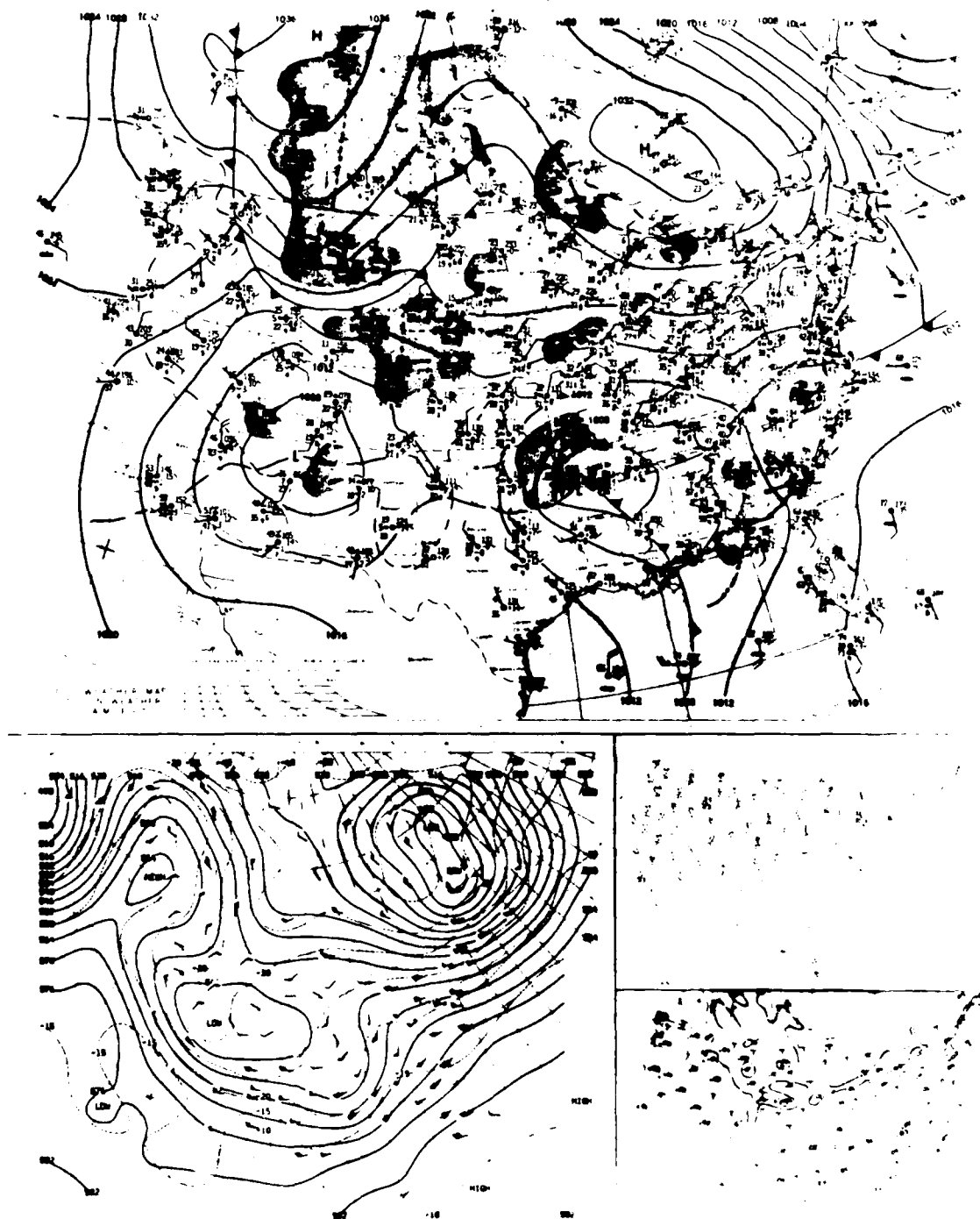
Figure 4.3   Same as Figure 4.1, except for 6 February 1986.
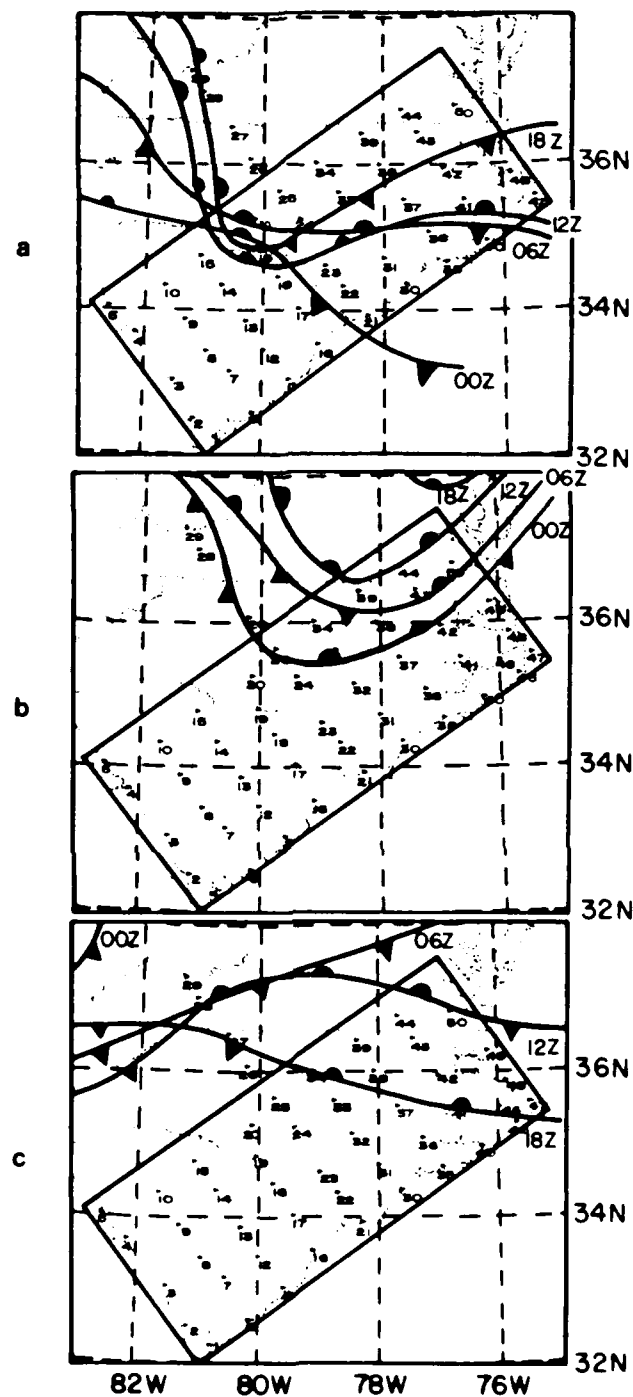
Figure 4.4 Position of front in GALE area at six-hourly
intervals for (a) 4 February 1986; (b) 5 February 1986;
(c) 6 February 1986.

24

5. GRAVITY WAVE CASES

Four gravity wave cases were identified during the three day observation period from the perturbation pressure field. For each of the cases, the perturbation pressure, filtered wind field (u and v components), filtered horizontal divergence, and hourly rainfall are shown (Figures 5.1-5.3, 5.5-5.10, 5.12-5.15, 5.17-5.22). The contour interval for the perturbation pressure is 0.2 mb. For the filtered wind field the maximum vector is 5.0 m s^{-1} as shown next to each plot. The horizontal divergence (δ) was calculated using:

$$\delta = \frac{\partial u}{\partial x} + \frac{\partial v}{\partial y} \tag{5.1}$$

where u and v are the *filtered horizontal wind* components. The derivatives in Equation 5.1 were calculated using centered finite differences. The value of the divergence for any point on the grid is multiplied by 10^{-6} and is in units of s^{-1}. The rainfall plot represents the total rainfall for the hour prior to the valid time. The contour interval is 1 mm for Cases 1, 3 and 4 and 2 mm for Case 2 (5 February). A larger contour interval was needed for Case 2 due to a large amount of precipitation occurring on that day. Table 5.1 summarizes wave parameters calculated directly from the surface plots.

25

Table 5.1 Gravity Wave Cases. Parameters were calculated using PAM II data only.

Case	Day (1986)	Time Period (GMT)	Orienta-tion	Movement	Speed (m s^{-1})	Wave-length (km)	Period (hr)	Amplitude (mb)
1	Feb 4	00-05	N-S	West to East	40	400	2.8	0.25-0.5
2	Feb 5	10-24	N-S	West to East	20-30	300-400	2.8-5.6	0.5-1.0
3	Feb 6	11-16	E-W	Southwest to Northeast	30-40	200-300	1.4-2.8	0.5-1.0
4	Feb 6	16-24	N-S	West to East	20-30	200-300	2.0-3.8	1.5-2.0

26

5.1 Case 1, 4 February 1986, Surface Data Analysis

On 4 February 1986, a weak gravity wave pattern moved through the GALE grid (Figures 5.1-5.3). This was initially identified on the perturbation pressure plots (Figures 5.1a - 5.3a) as a north-south oriented wave moving from west to east. At 0120 GMT (Figure 5.1a), there was an axis of high pressure at the upper left of the grid and an axis of low pressure approximately mid-way through the grid. By 0220 GMT (Figure 5.2a), the wave had moved with a phase speed of approximately 40 m s^{-1}. At 0330 GMT (Figure 5.3a), the pattern was not as well defined, but movement continued to the east. From the perturbation pressure plots, the wavelength was approximately 400 km, with a period of 2.8 hours. The amplitude was between 0.25 to 0.5 mb. These are summarized in Table 5.1 and compared with the other cases.

At 0120 GMT, the wind and horizontal divergence plots (Figures 5.1 b-c) snow well-defined areas of convergence and divergence. There does appear to be movement of these fields to the east (Figures 5.2 b-c and 5.3 b-c), following the movement of the wave though the pattern becomes less well-defined. There also was no rainfall associated with this occurrence of gravity waves.

From the perturbation pressure plots versus time for stations 19 and 38 (Figure 5.4), the time interval for

27

Figure 5.1 PAM II Data (a) perturbation pressure;
(ᴅ) filtered winds; (c) filtered horizontal divergence;
(d) hourly rainfall for Case 1, 4 February 1986 at 0120
GMT. See text for details.
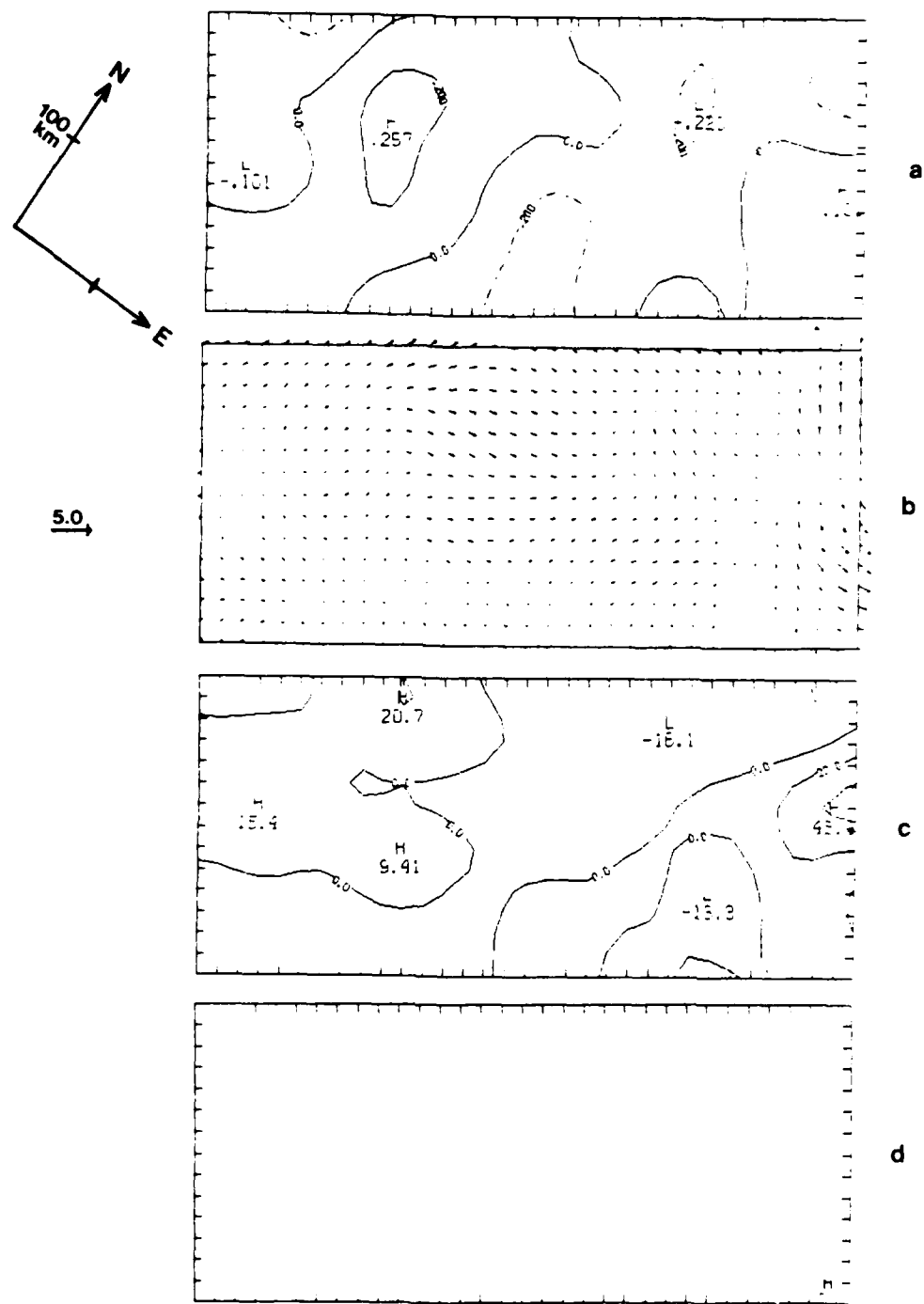
Figure 5.2   Same as Figure 5.1, except for a valid time of 0220 GMT.
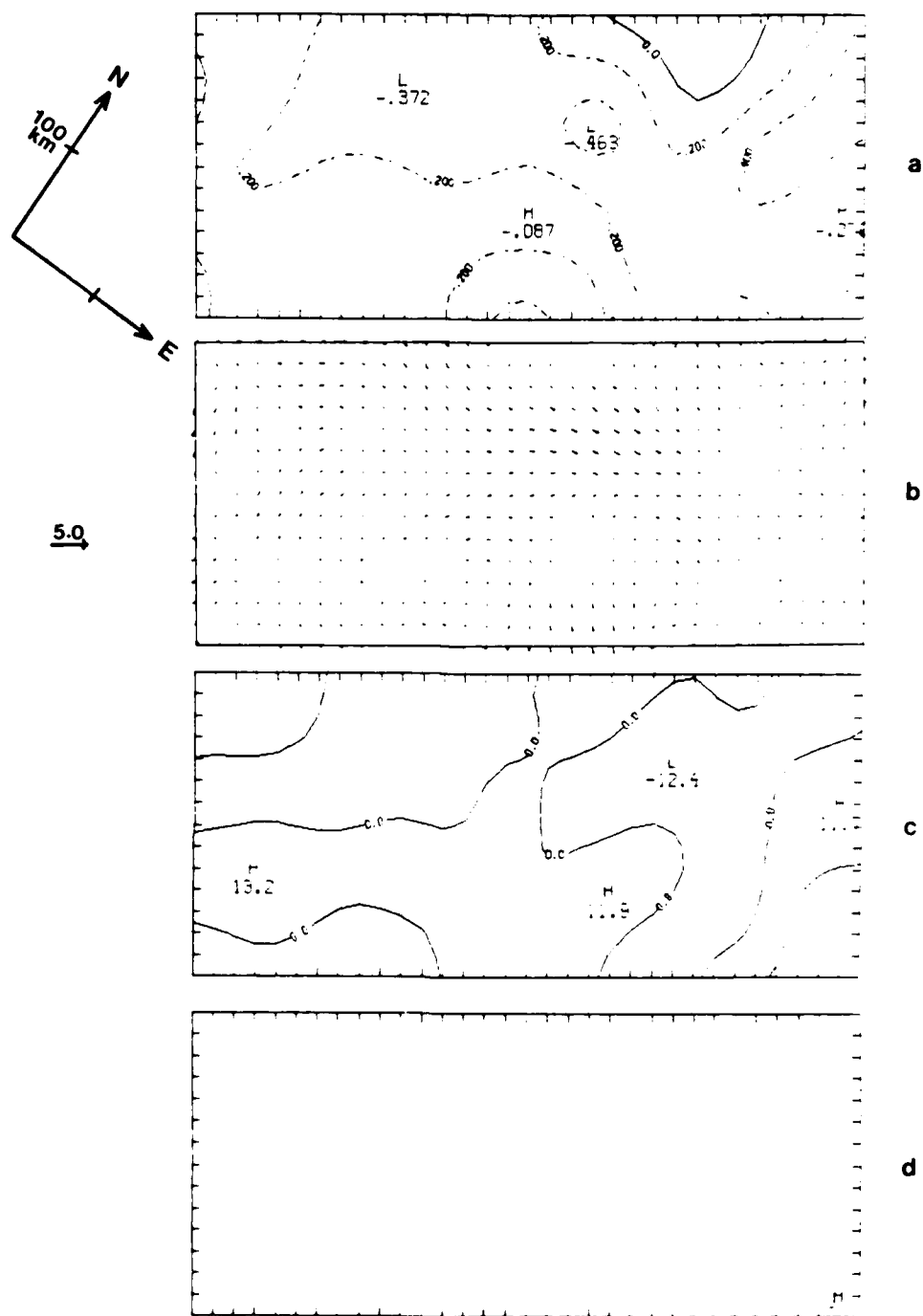
Figure 5.3   Same as Figure 5.1, except for a valid time of
0330 GMT.
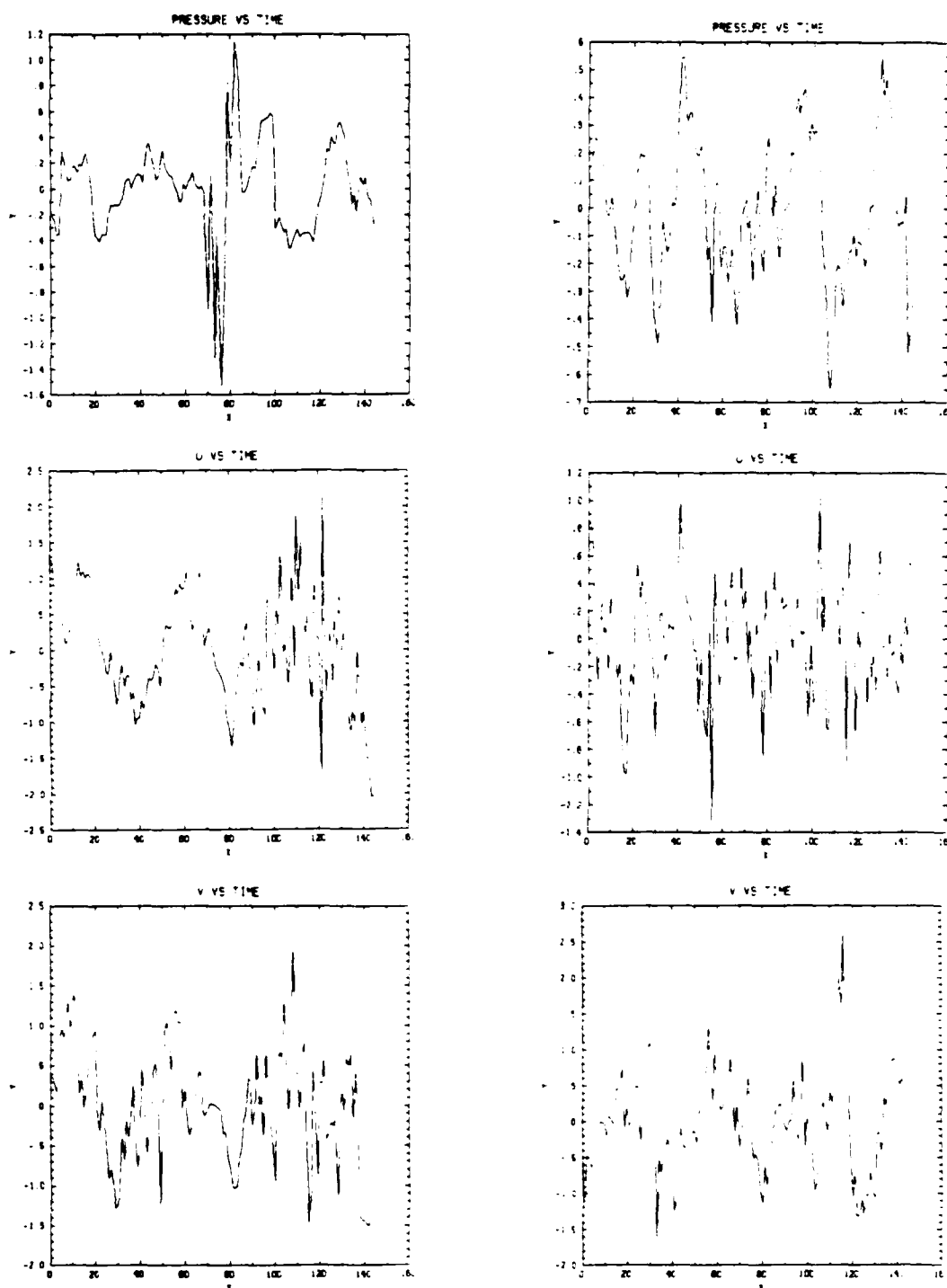
Figure 5.4   Perturbation pressure (y) versus time (x);
u and v components of the filtered wind in m s^{-1} (y) versus
time (x) for station 19 (left) and station 38 (right) on 4
February 1986.   Time is in 10-minute intervals.

31

gravity wave passage was between 9 and 21. These plots can be used to make another estimate of the wave amplitude. By halving tne value from the highest perturbation pressure to the lowest during the observation time, a second estimate of the amplitude is approximately 0.25 mb. Station 19 showed an increased u component of the wind while the v component decreased (Figure 5.4). Station 38 showed more variability in the wind, including a change in direction, during the observation time (Figure 5.4).

Figure 5.4 shows many other larger amplitude oscillations during this day. However, during later times, there was no evidence of spatially coherent patterns associated with these oscillations. These may have been associated with gravity waves with wavelengths smaller than the station spacing.

5.2 Case 2, 5 February 1986, Surface Data Analysis

At 1500 GMT on 5 February 1986, a wave began to appear in tne upper left corner of the grid (Figure 5.5a). By 1600 GMT (Figure 5.6a), tne wave was much more pronounced and continued to move to the east. It remained on an easterly track tnrough 1700 GMT (Figure 5.7a) and by 1800 GMT (Figure 5.8a), there appeared to be a second wave entering the grid moving from the west. Both waves continued easterly (Figures 5.9a and 5.10a) with phase speeds from 20 to 30 m s^{-1} and wavelengths between 300 to 400 km

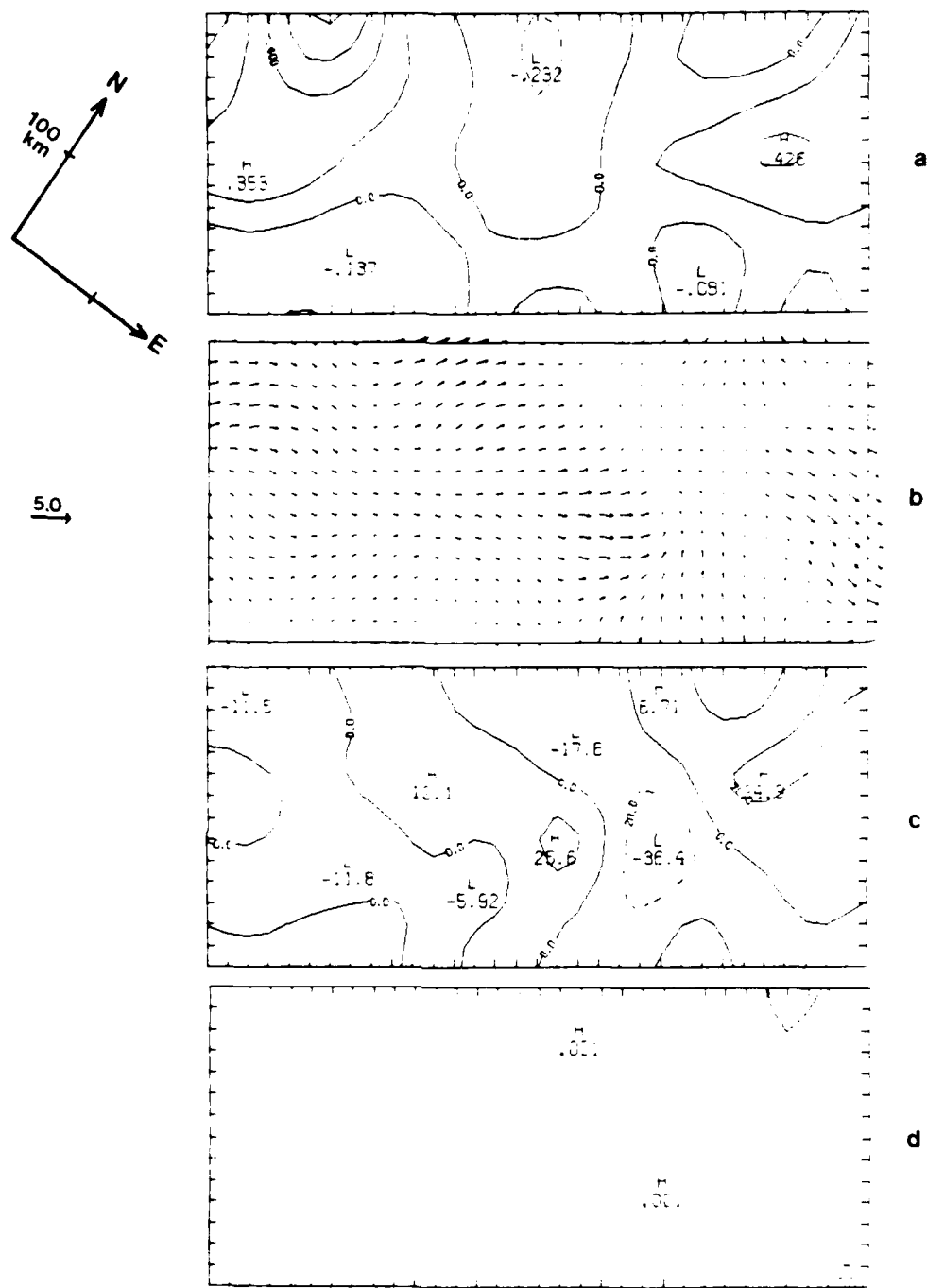Figure 5.5   PAM II Data   (a) perturbation pressure;
(b) filtered winds; (c) filtered horizontal divergence;
(d) hourly rainfall for Case 2, 5 February 1986 at 1500
GMT.   See text for details.

33
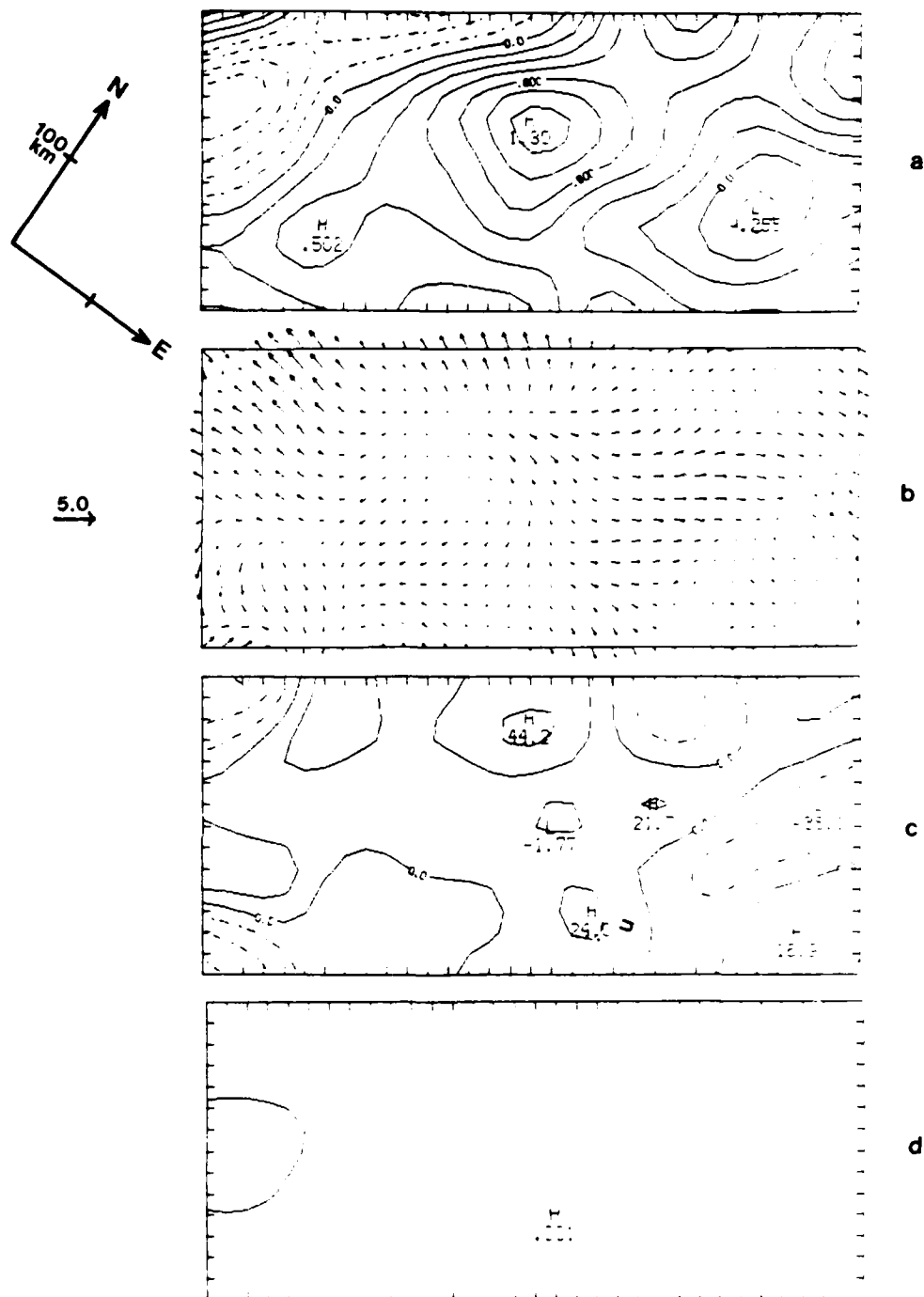
Figure 5.6   Same as Figure 5.5, except for a valid time of 1600 GMT.
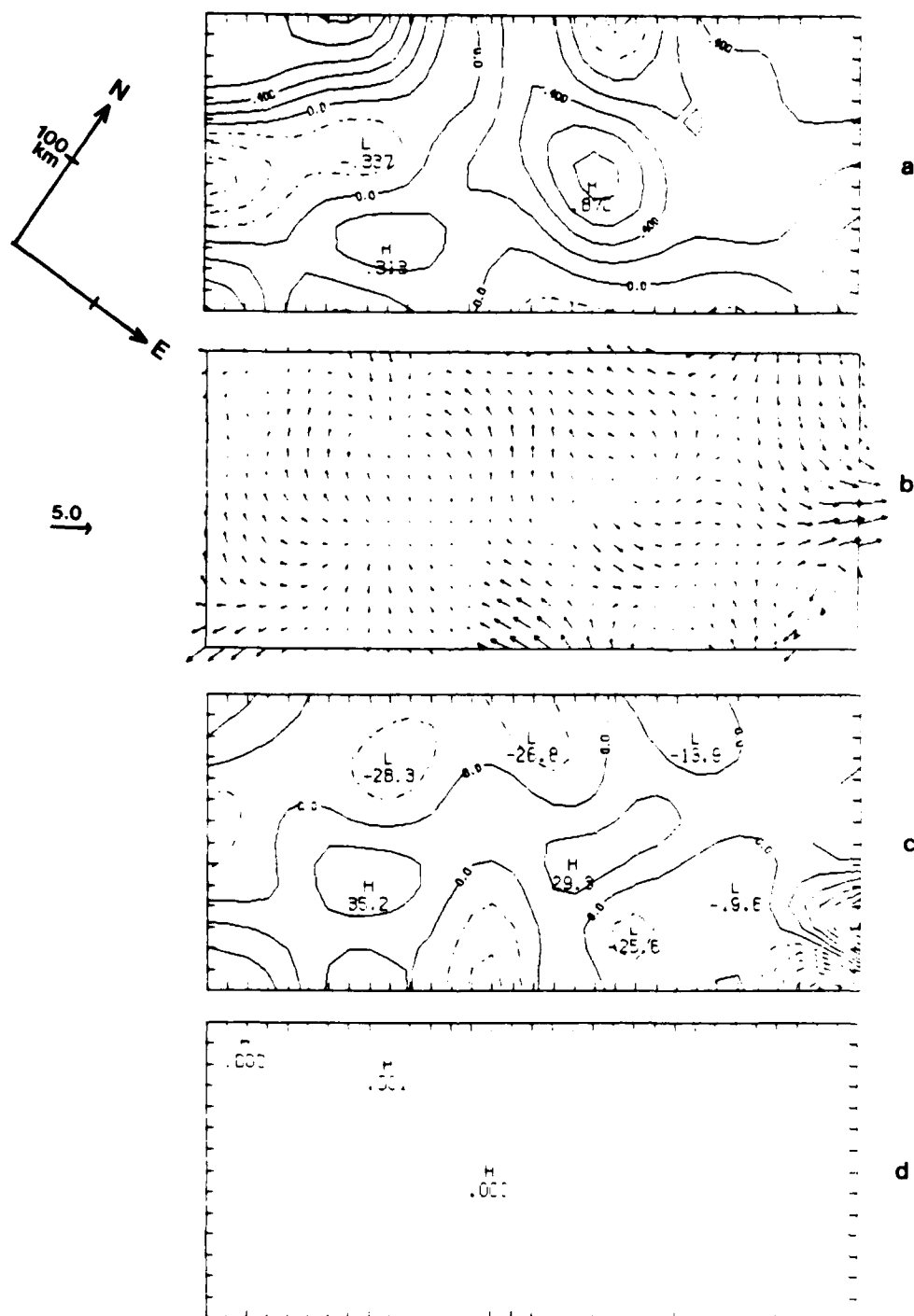
Figure 5.7   Same as Figure 5.5, except for a valid time of
1700 GMT.
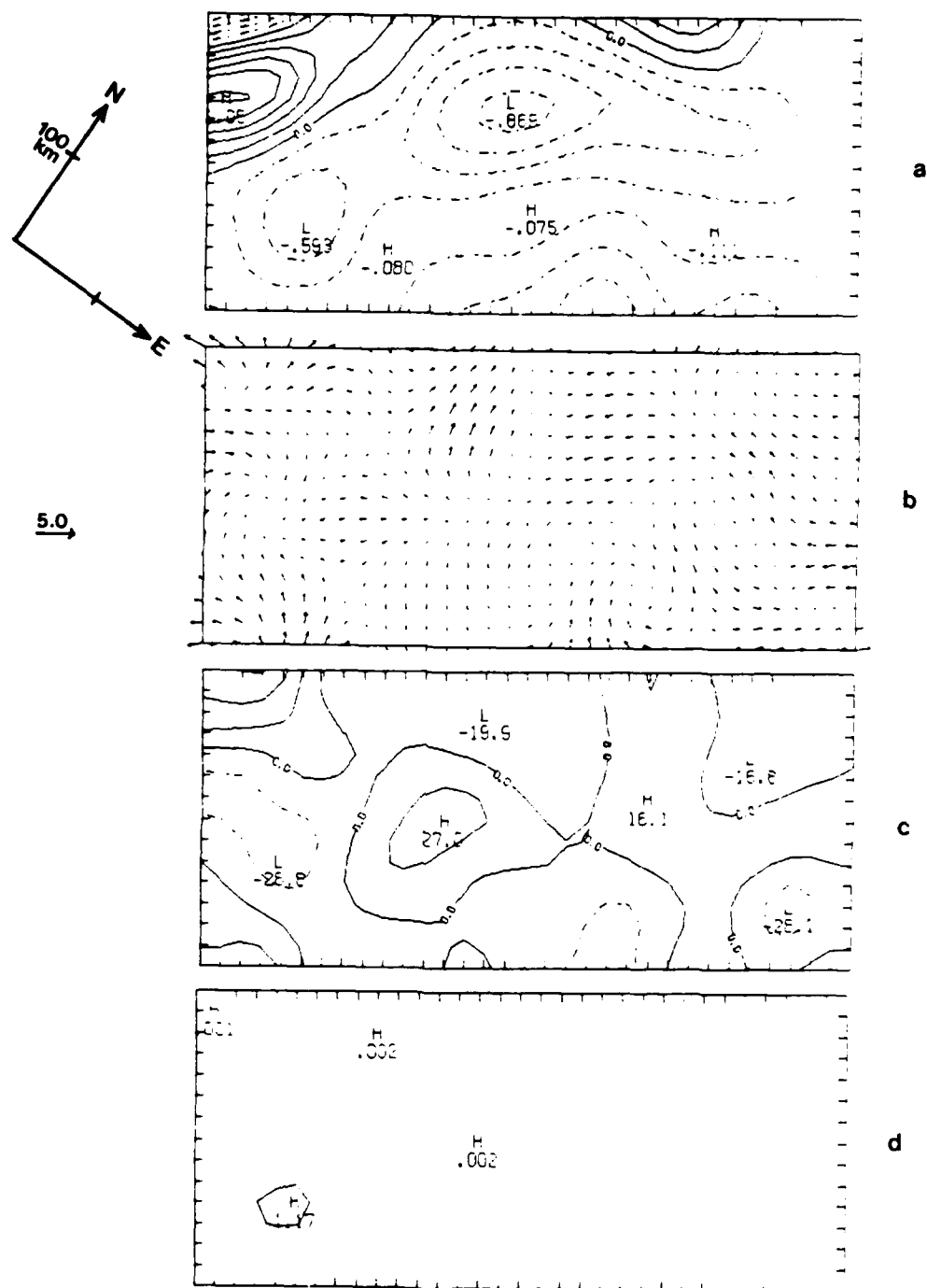
Figure 5.8   Same as Figure 5.5, except for a valid time of 1800 GMT.

Figure 5.9   Same as Figure 5.5, except for a valid time of
1900 GMT.

Figure 5.10 Same as Figure 5.5, except for a valid time of 2000 GMT.

(Table 5.1). Periods were calculated as 2.3 - 5.6 hours and amplitudes ranged from 0.5 - 1.0 mb.

From the wind and horizontal divergence fields (Figures 5.5 b-c through 5.10 b-c) a pattern of divergence preceded the movement of both waves. At 1500 GMT, there was approximately 18 mm of rainfall measured for the prior hour in the northeast corner of the grid (Figure 5.5d). For the next 4 hours (Figures 5.6d - 5.9d), there were very isolated cases of precipitation of almost insignificant amounts. But at 2000 GMT, approximately 46 mm of rain was measured (Figure 5.10d) though again, this might have been an isolated rainshower. Thus, the gravity wave may have triggered precipitation, but did not appear to have continuous precipitation moving with it. Figure 5.11 shows the perturbation pressure plots for stations 8 and 18. The time of interest is 91 to 121. During this period, a significant decrease occurs as both waves pass the station. Amplitudes for the waves are approximately 1 mb. Both stations showed great variability in the wind (Figure 5.11) during the observation period with changes in speed and direction.

5.3 Case 3, 6 February 1986, Surface Data Analysis

Case 3 was different from the others in that it appeared on the grid with an east-west orientation at approximately 1200 GMT (Figure 5.12a) and moved from the

Figure 5.11   Perturbation pressure (y) versus time (x); u and v components of the filtered wind in m s^{-1} (y) versus time (x) for station 8 (left) and station 18 (right) on 5 February 1986.   Time is in 10-minute intervals.

40
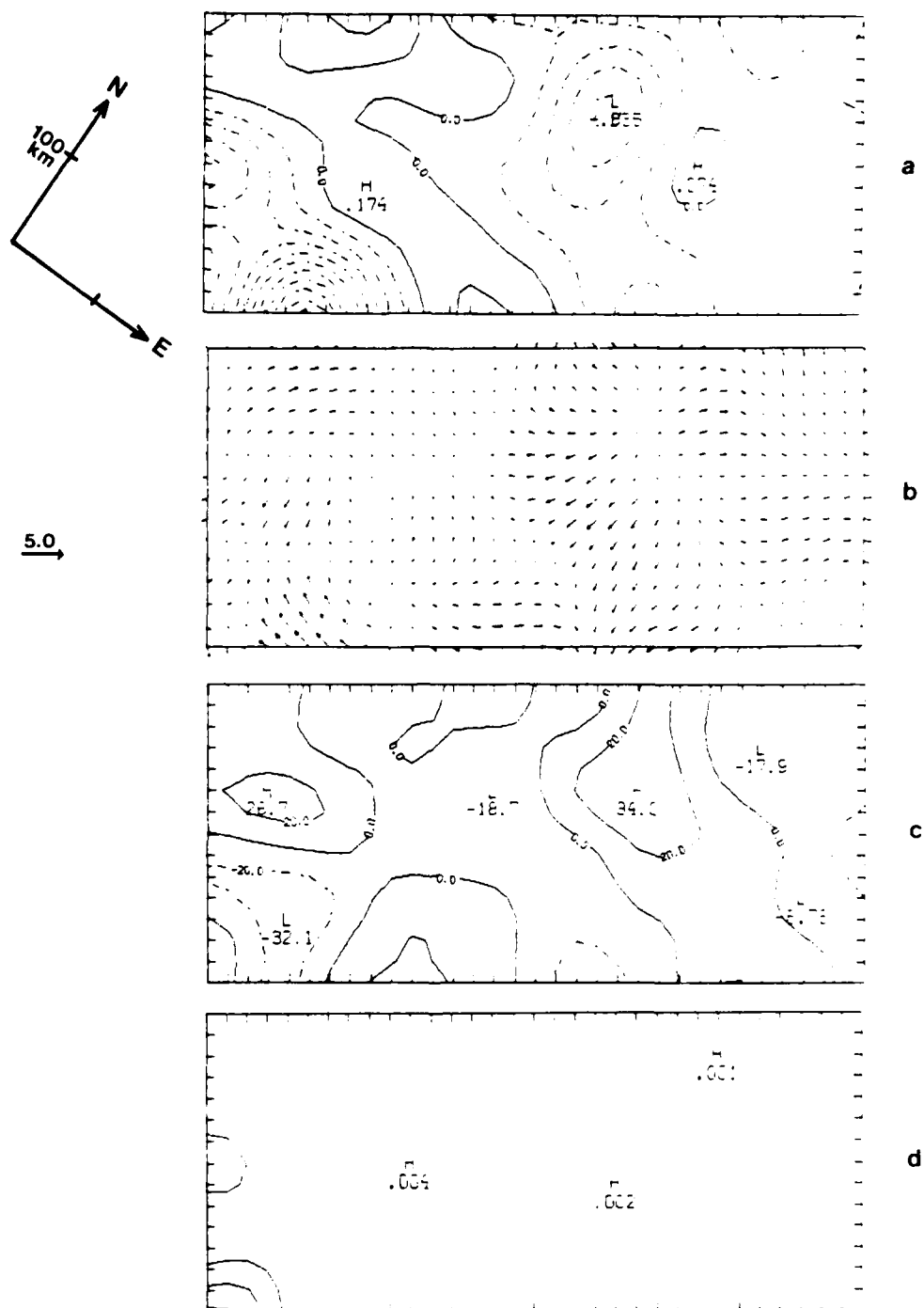
Figure 5.12 PAM II Data (a) perturbation pressure;
(b) filtered winds; (c) filtered horizontal divergence;
(d) hourly rainfall for Case 3, 6 February 1986 at 1200
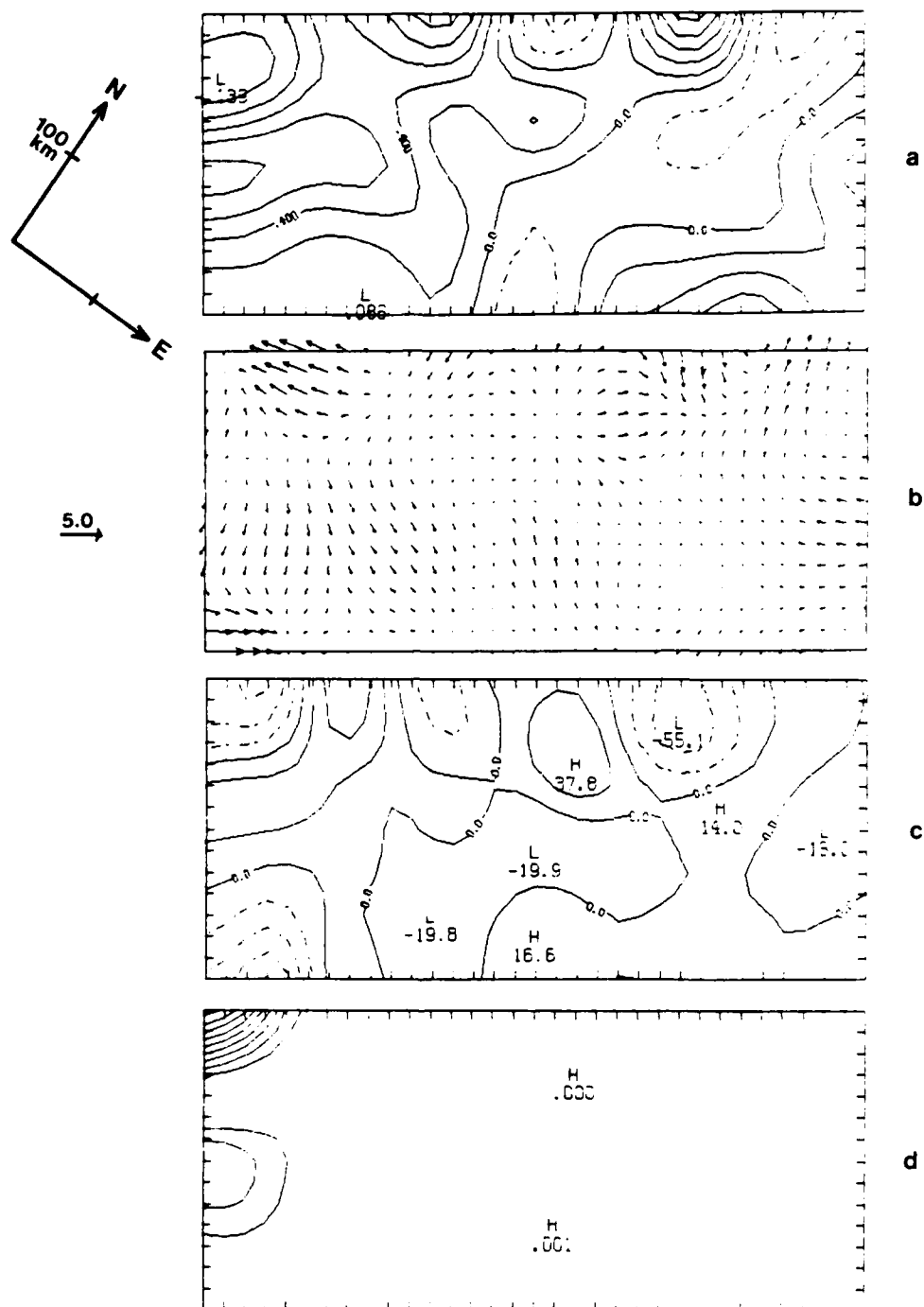GMT. See text for details.

41

southwest to the northeast (Figures 5.13a - 5.15a). The phase speed was estimated to range from 30 - 40 m s^{-1} with a wavelength from 200 - 300 km (Table 5.1). The period was calculated to be 1.4 - 2.8 hours, with an amplitude of 0.5 - 1.0 mb.

The wind and horizontal divergence plots (Figures 5.12 b-c through 5.15 b-c), though quite diffuse, seemed to indicate divergence preceding the gravity wave. In Case 3, precipitation continued to be measured in the bottom left corner of the grid for the entire period (Figures 5.12d through 5.15d).

On the single station plots in Figure 5.16, the observation time interval is 73 - 91. The amplitude calculated from the perturbation pressure plots of both stations range from 0.5 - 0.8 mb. Both stations also showed significant changes in both wind speed and direction during that time (Figure 5.16).

5.4 Case 4, 6 February 1986, Surface Data Analysis

Case 4 was the most well-defined of all the four cases. As can be seen at 1800 GMT (Figure 5.17a), a linear wave oriented north-to-south had entered the grid from the west. As it continued moving eastward (Figures 5.18a through 5.22a) with a phase speed of about 20 - 30 m s^{-1} it did not lose much of its linear form. The horizontal divergence plots showed areas of convergence and divergence

42
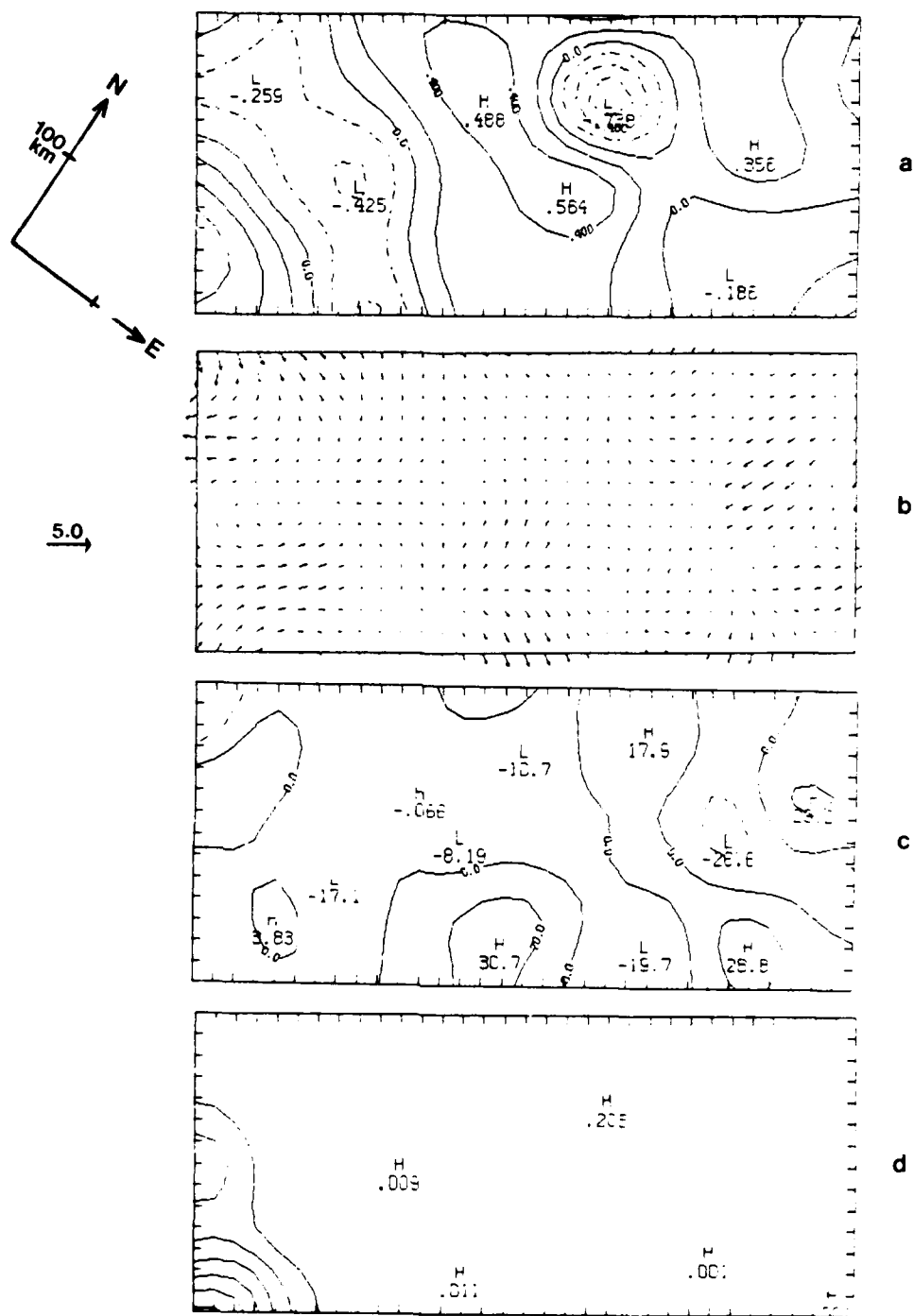
Figure 5.13   Same as Figure 5.12, except for a valid time of 1300 GMT.
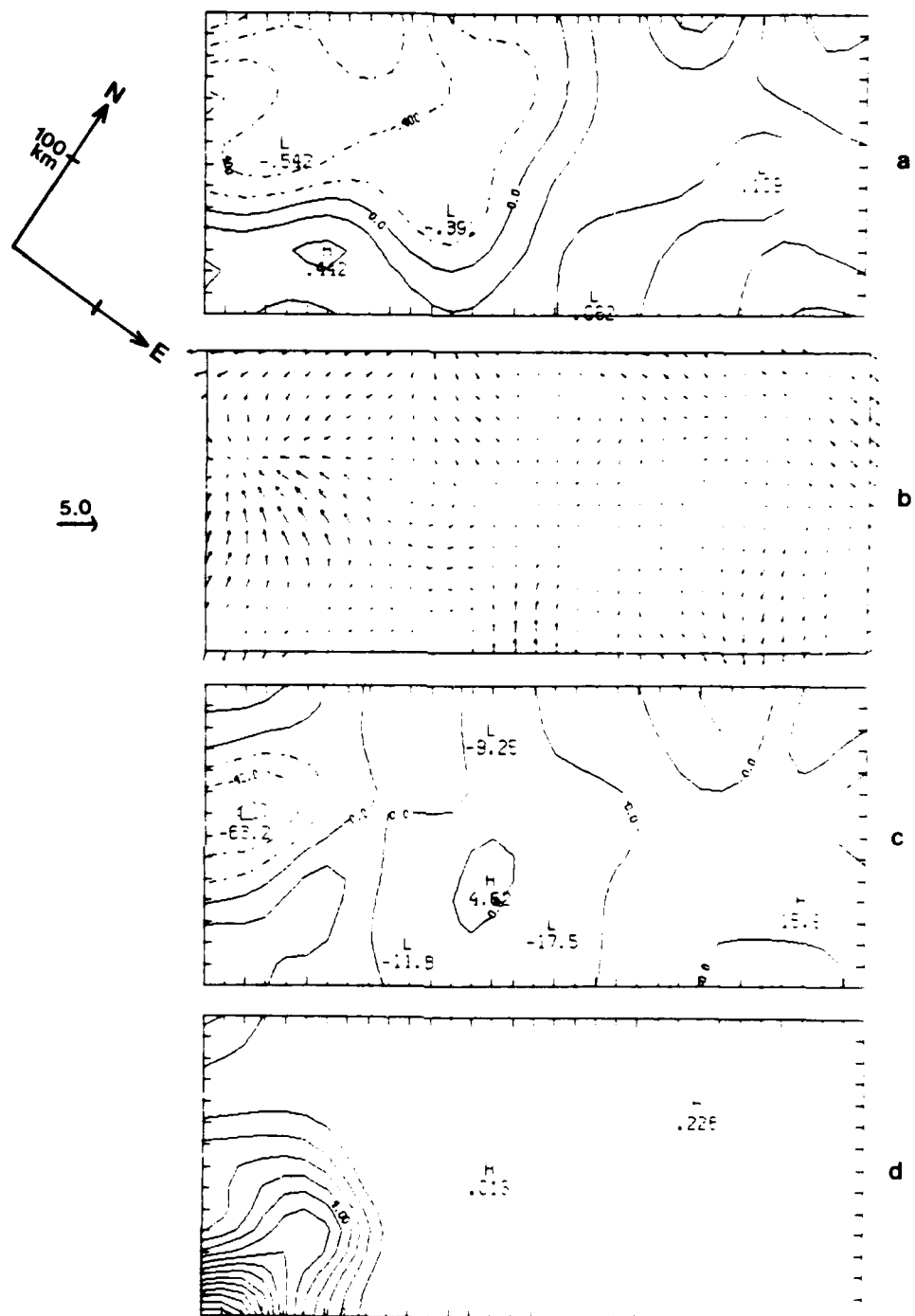
Figure 5.14   Same as Figure 5.12, except for a valid time
of 1400 GMT.

44
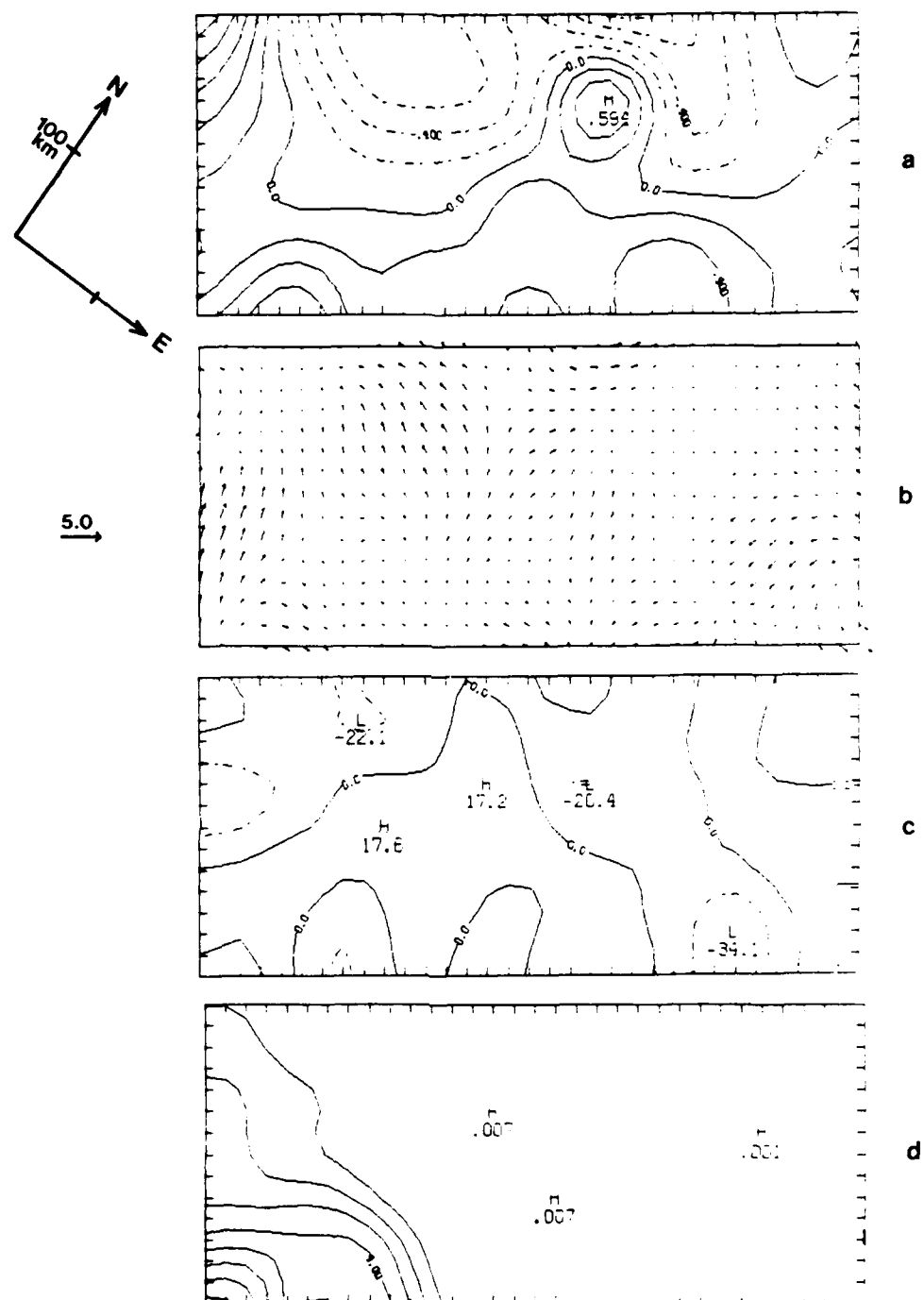
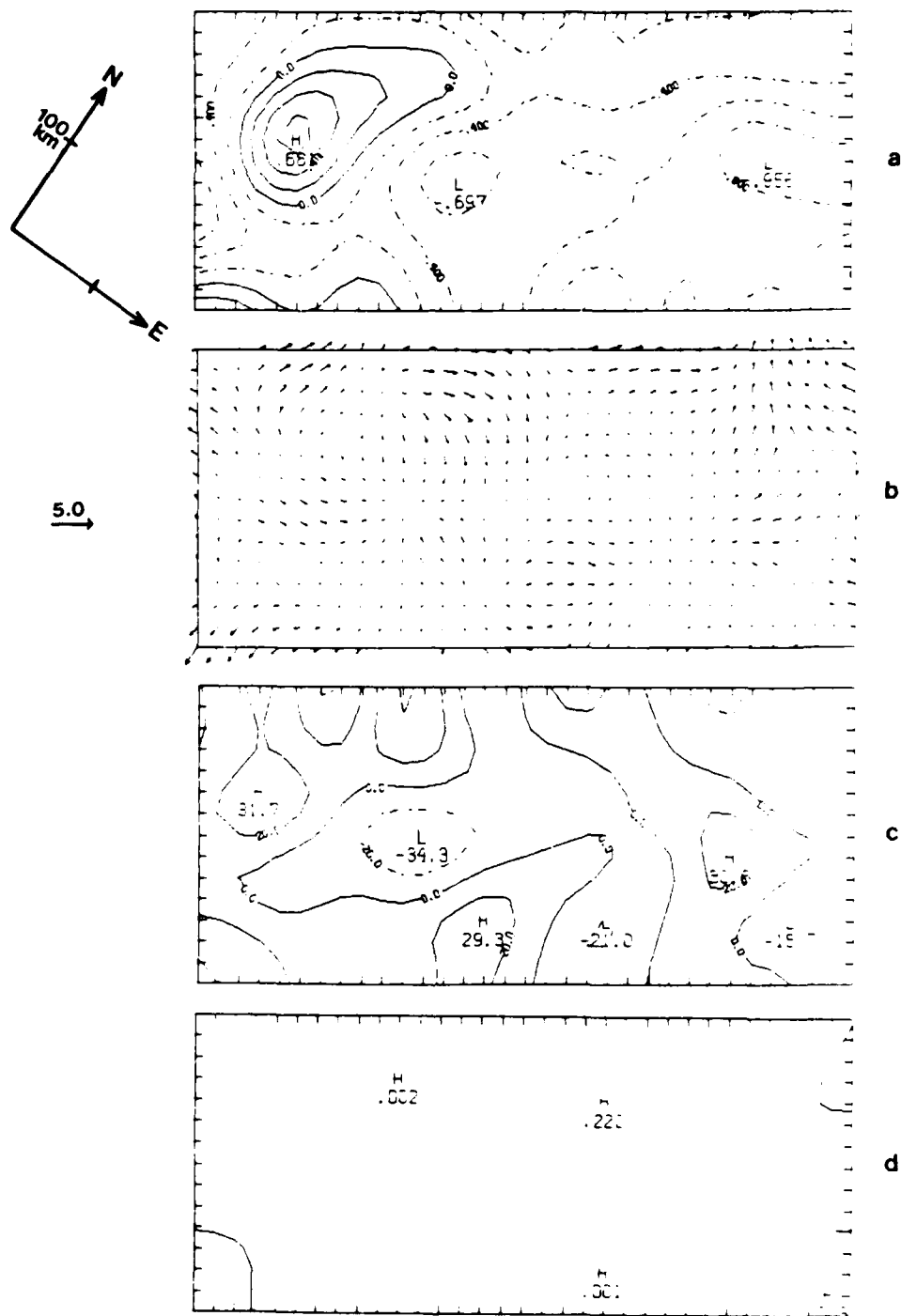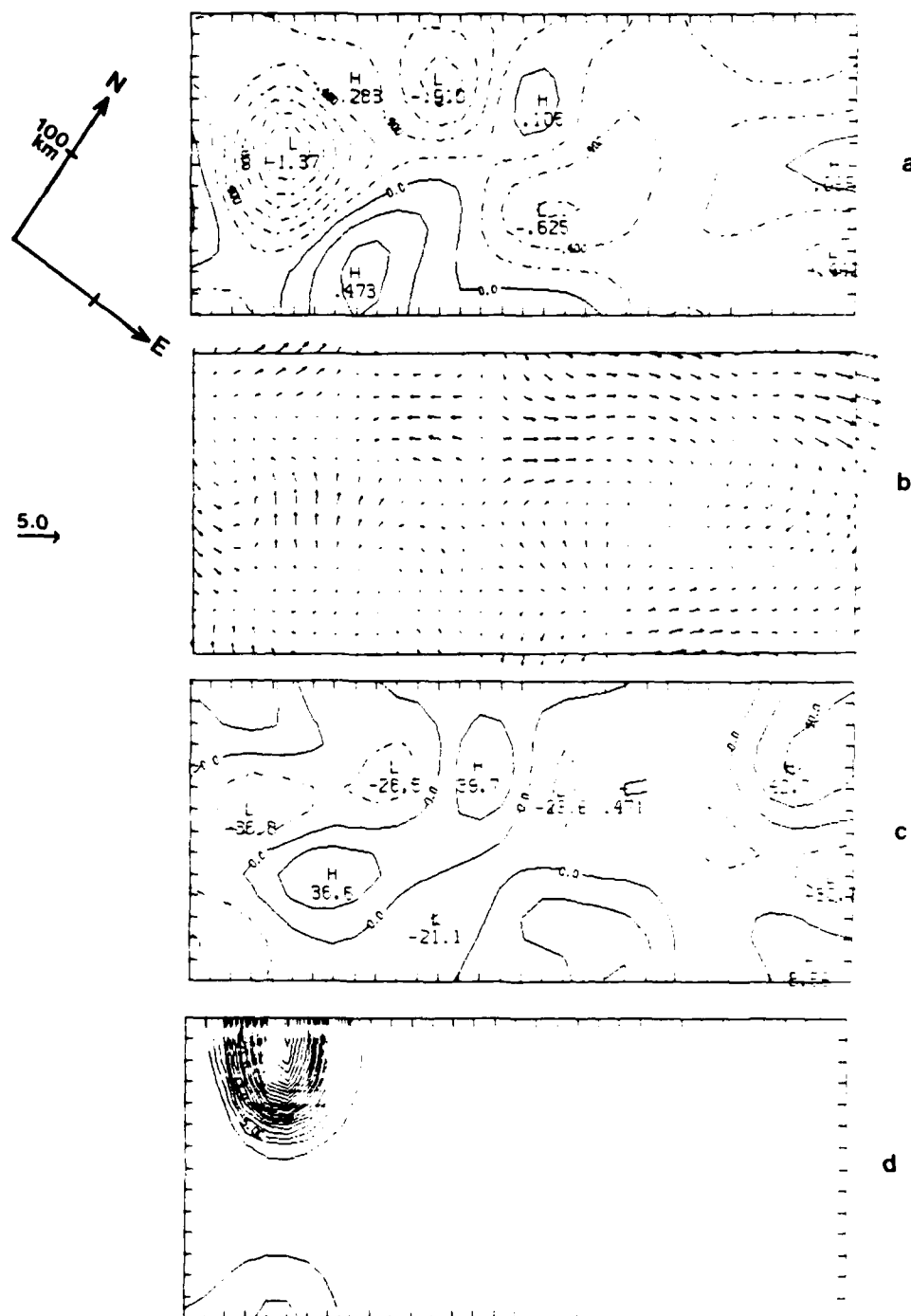Figure 5.15   Same as Figure 5.12, except for a valid time of 1500 GMT.
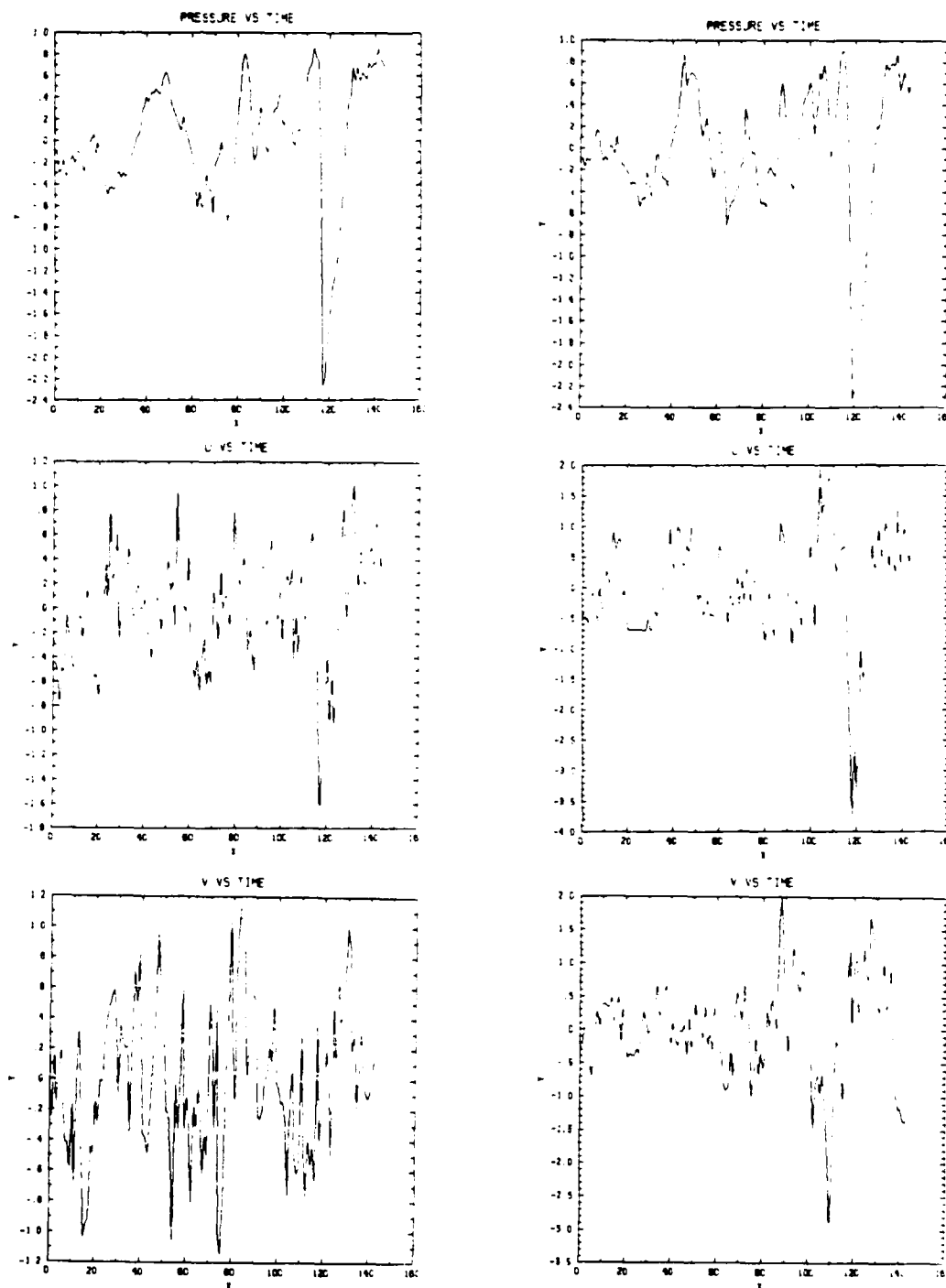
Figure 5.16 Perturbation pressure (y) versus time (x); u and v components of the filtered wind in m s^{-1} (y) versus time (x) for station 7 (left) and station 13 (right) on 6 February 1986. Time is in 10-minute intervals.

46
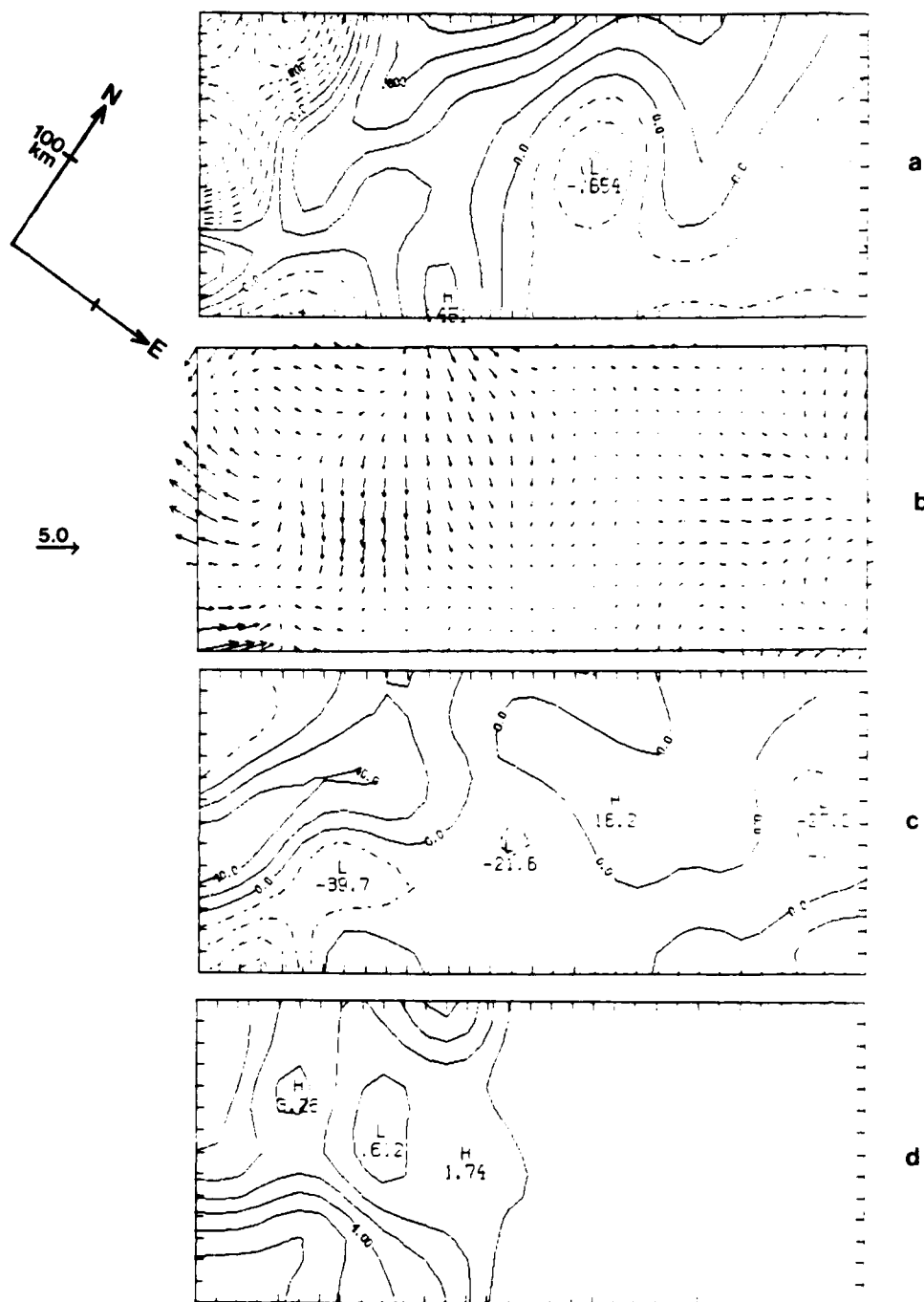
Figure 5.17 PAM II Data (a) perturbation pressure;
(b) filtered winds; (c) filtered horizontal divergence;
(d) hourly rainfall for Case 4, 6 February 1986 at 1800
GMT. See text for details.

47
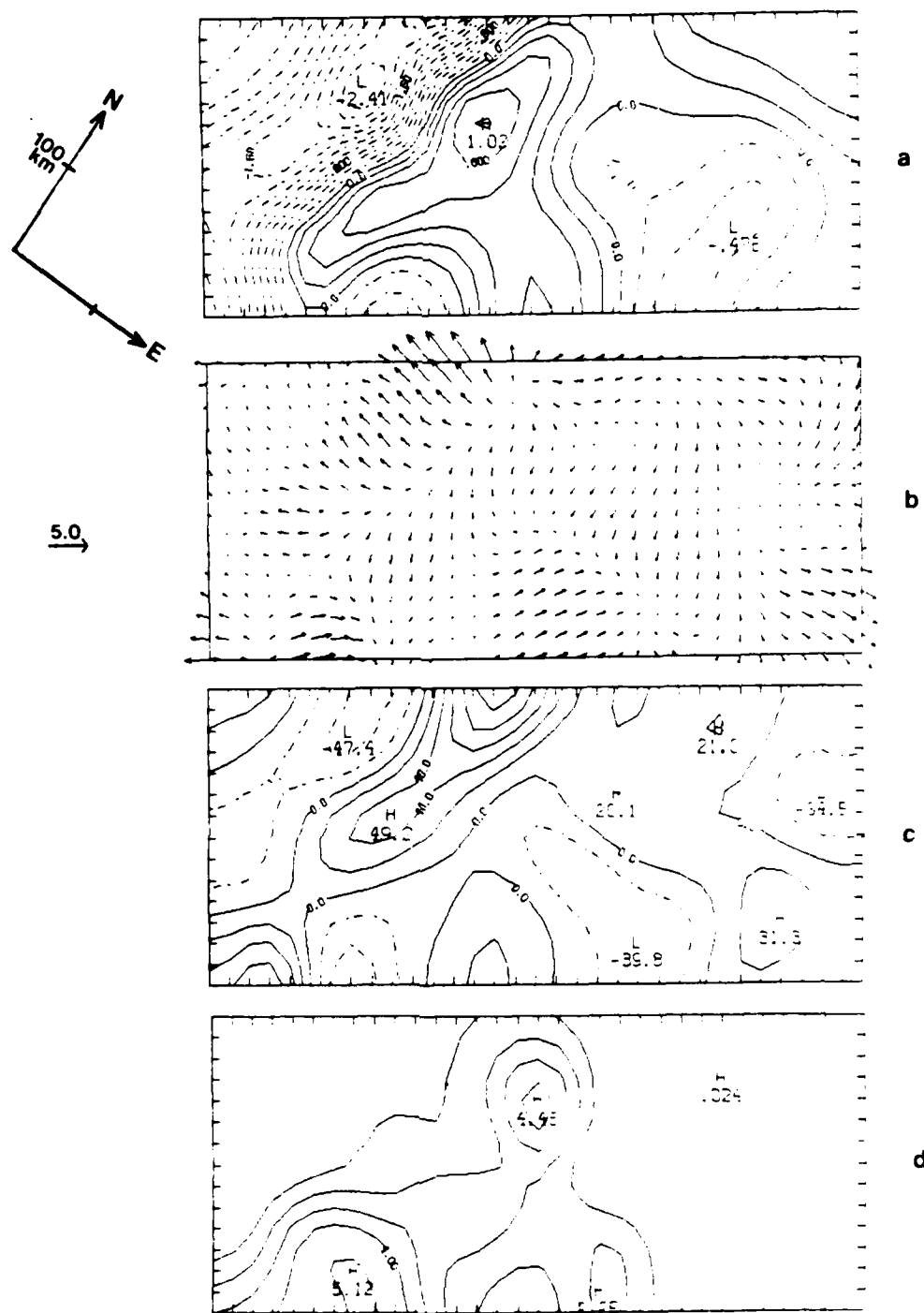
Figure 5.18   Same as Figure 5.17, except for a valid time
of 1900 GMT.

48
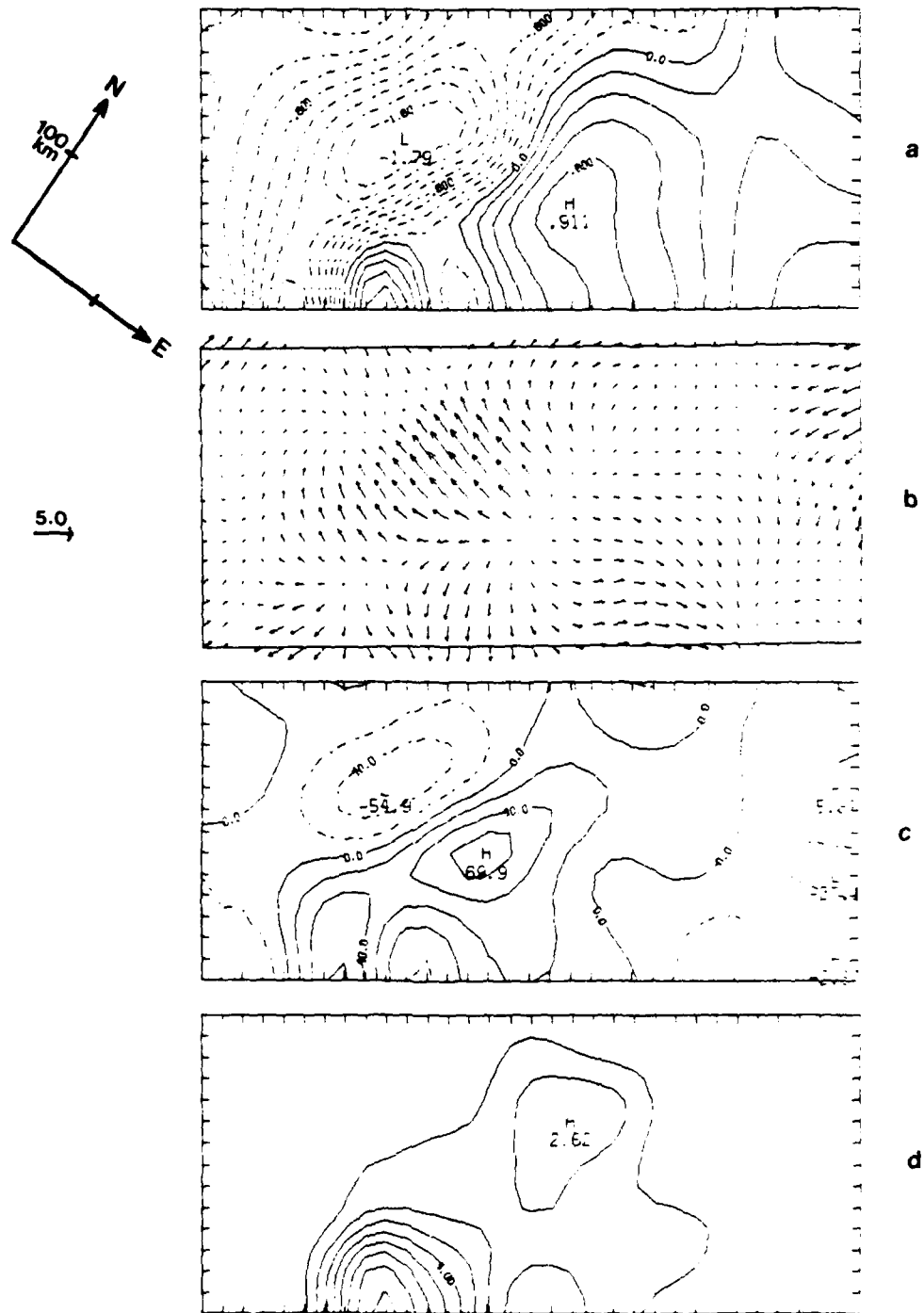
Figure 5.19 Same as Figure 5.17, except for a valid time of 2000 GMT.

49
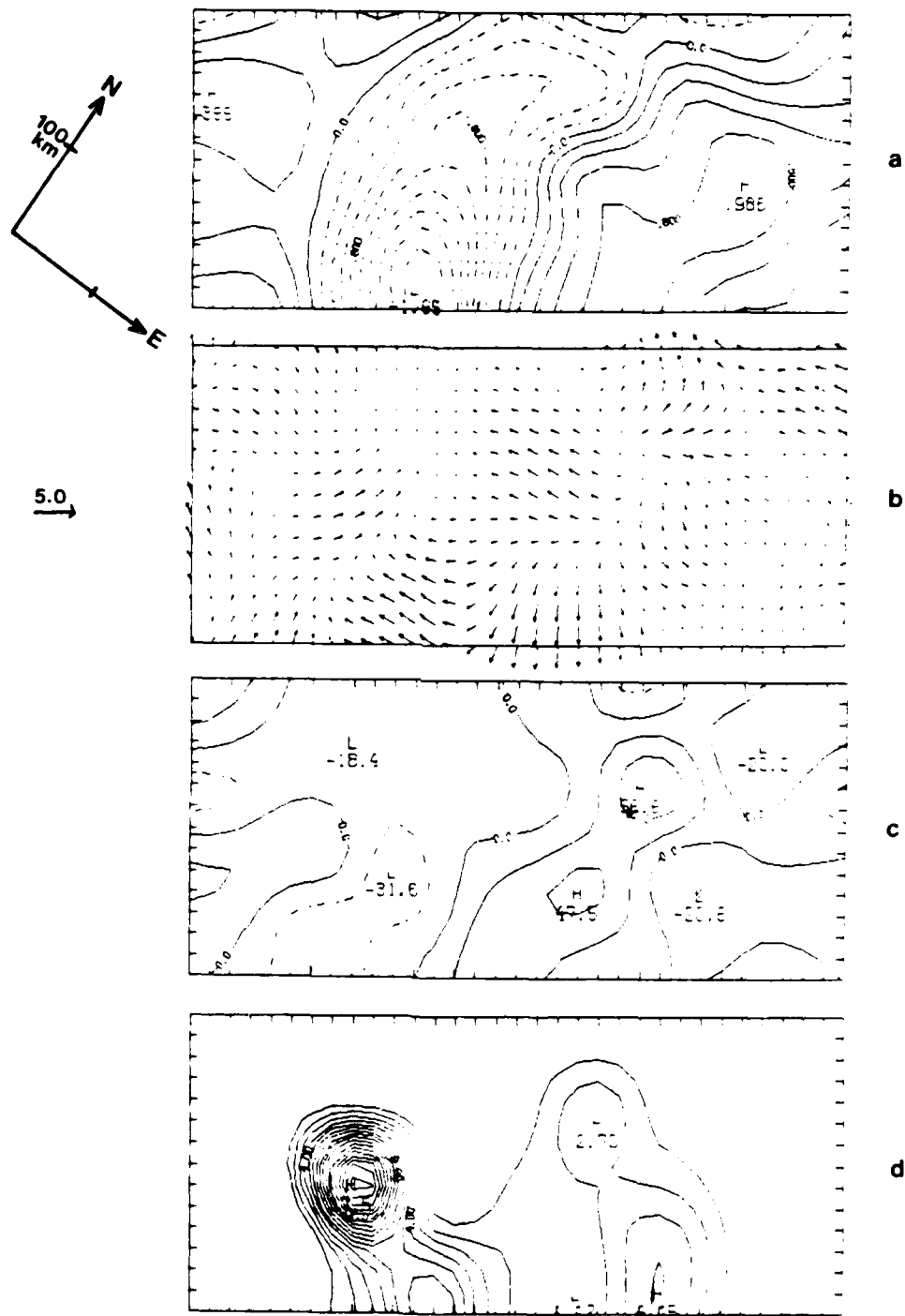
Figure 5.20 Same as Figure 5.17, except for a valid time
of 2100 GMT.

50
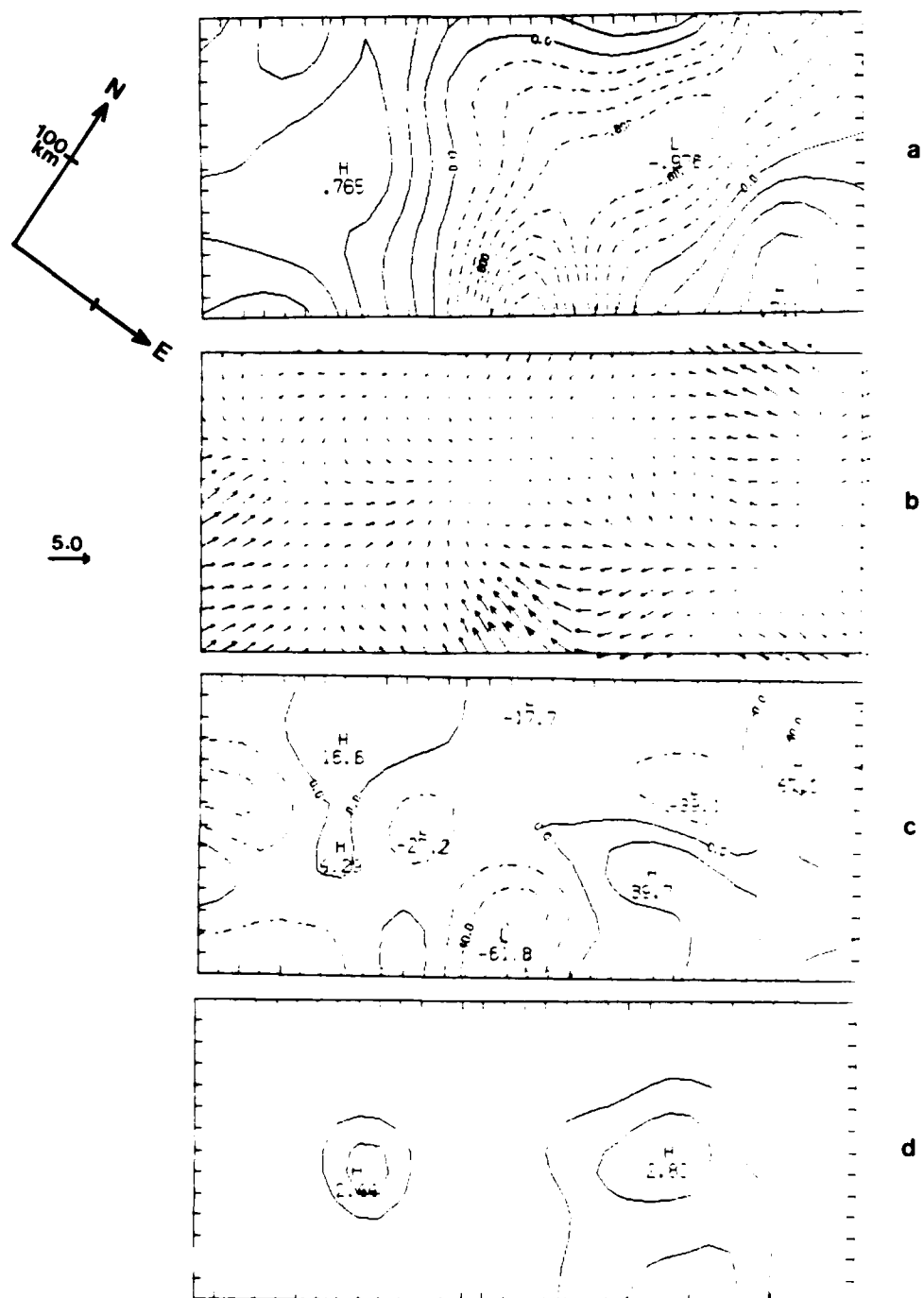
Figure 5.21 Same as Figure 5.17, except for a valid time of 2200 GMT.
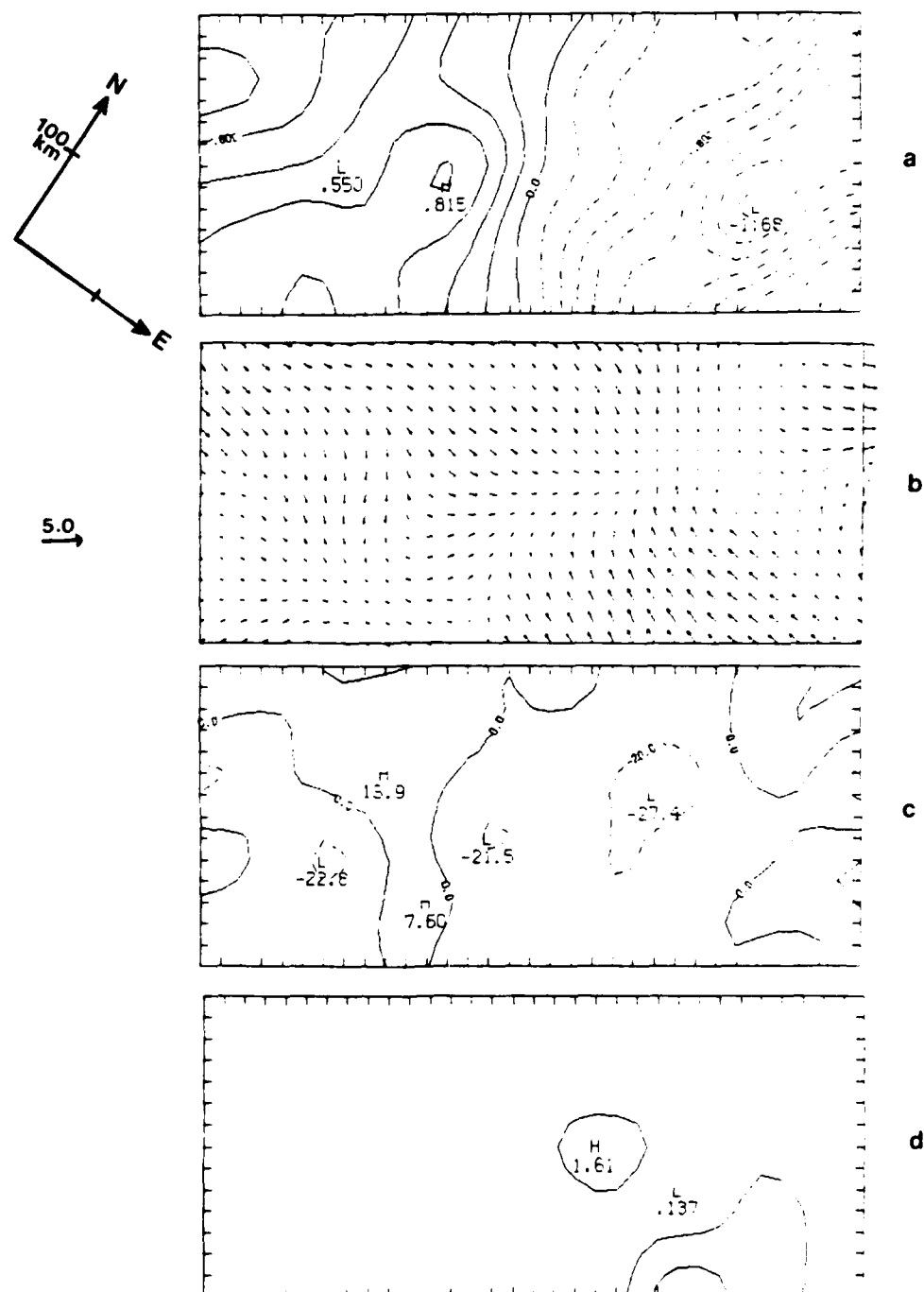
Figure 5.22   Same as Figure 5.17, except for a valid time
of 2300 GMT.

moving exactly with the wave (Figures 5.18c through 5.22c).
Once again, divergence preceded the wave. This area of
convergence and divergence is associated with the perturba-
tion wind which is blowing almost directly down the
pressure gradient in the vicinity of the wave (Figures
5.18c-5.22c). The hourly rainfall also showed very good
correlation with the wave motion (Figures 5.18d through
5.22d). As the wave moved east, so did the precipitation.

Stations 18 and 32 showed very significant decreases
in perturbation pressure during the time interval from
109 - 139 (Figure 5.23). Amplitudes range from 1.2 - 1.5
mb. Both stations showed the u and v component of the wind
changing in both speed and direction (Figure 5.23).

An interesting feature of this wave is that its struc-
ture remained almost constant as it moved across the entire
domain. In Cases 1 and 3, the pattern was difficult to
follow after it crossed about half of the domain. In Case
2 there appeared to be a group of waves which resulted in a
very complicated structure.

For all four cases, the perturbation temperature field
showed no spatially coherent patterns. The vorticity was
calculated from the filtered winds and like the perturba-
tion temperature, did not have any identifiable features
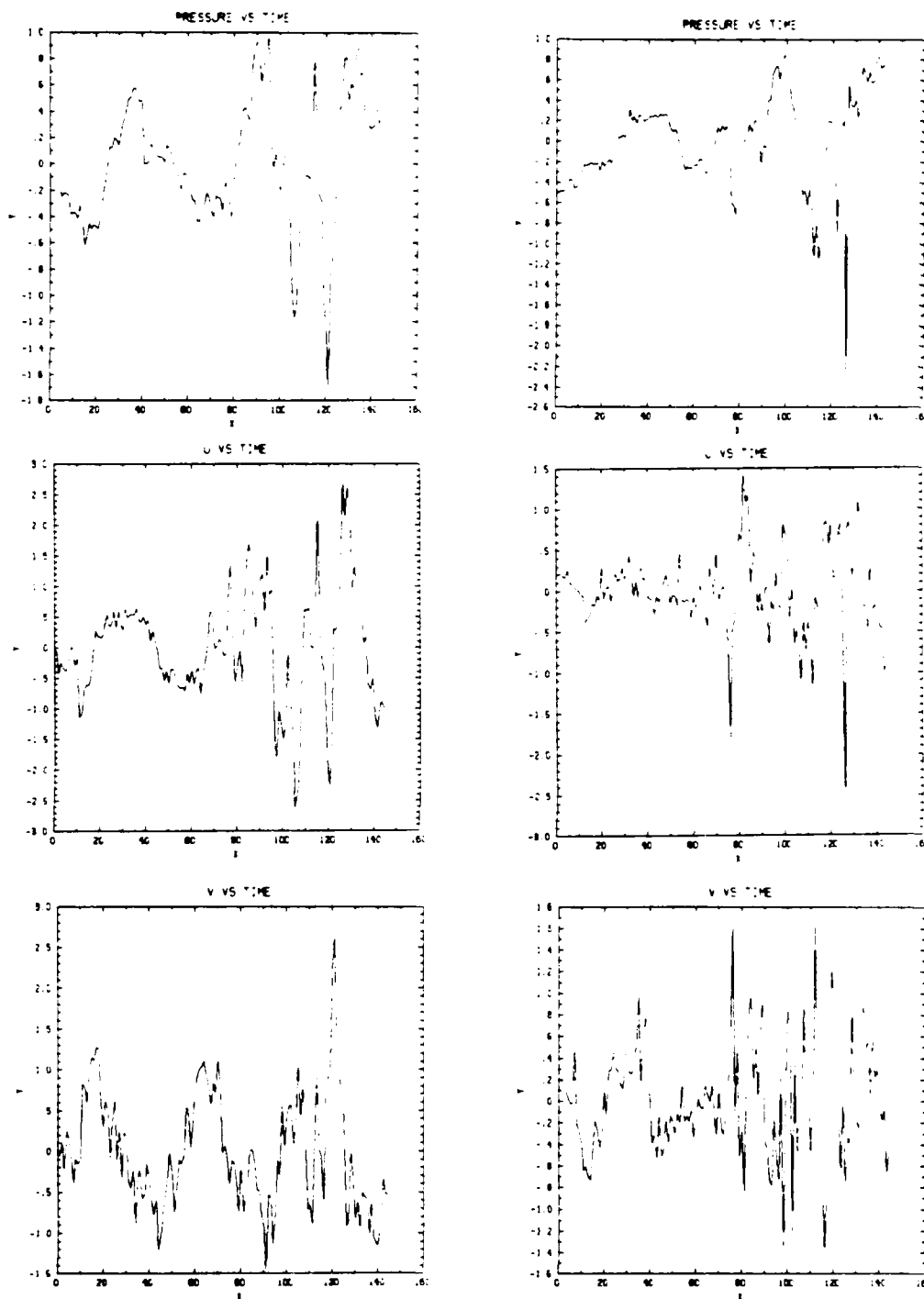associated with it.
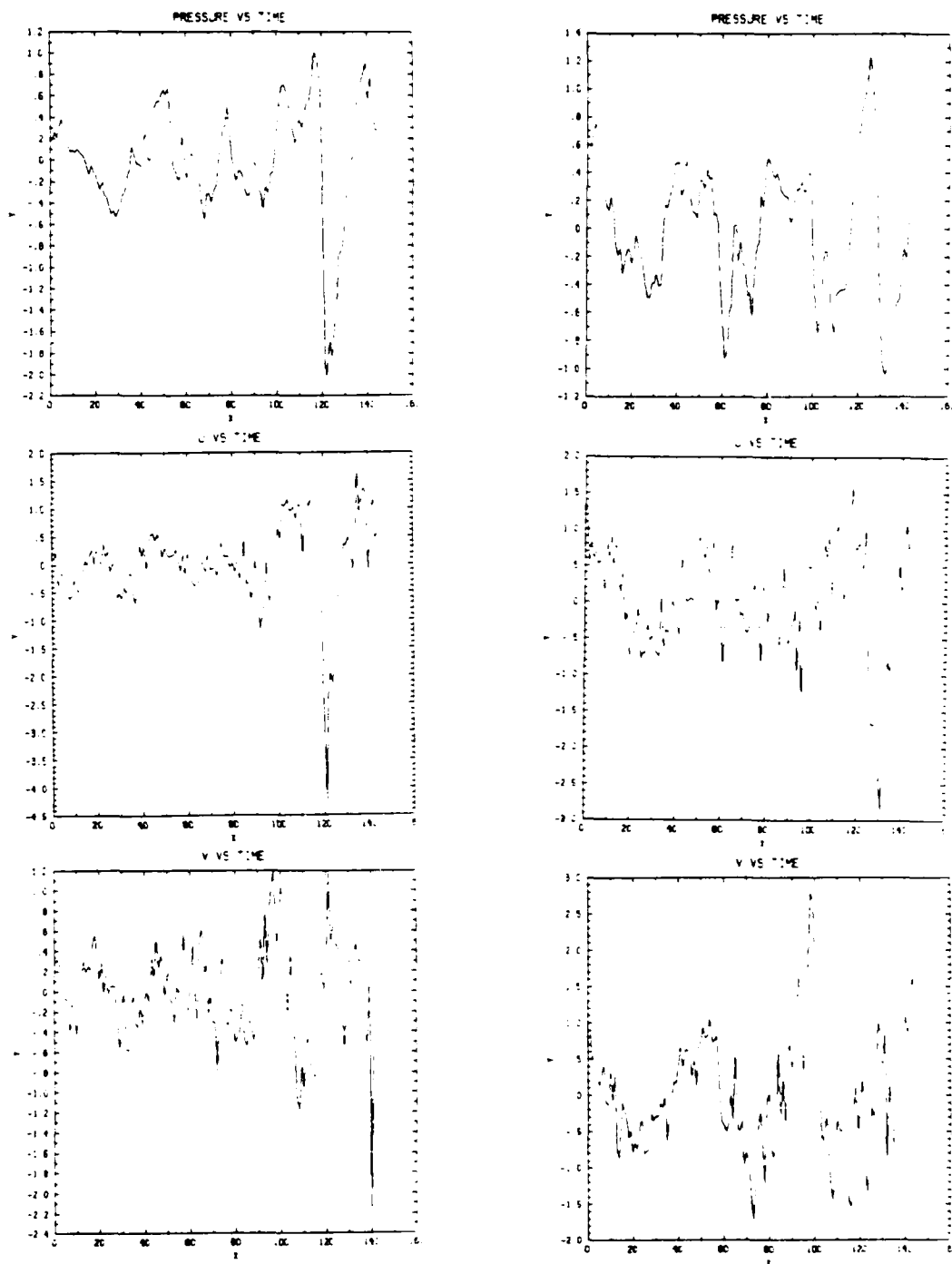
Figure 5.23 Perturbation pressure (y) versus time (x); u and v components of the filtered wind in m s^{-1} (y) versus time (x) for station 18 (left) and station 32 (right) on 6 February 1986. Time is in 10-minute intervals.

6. COMPARISON OF CASE STUDY - RESULTS WITH THEORY

In order to further analyze the four gravity wave cases, sounding data were also used. For this purpose, the two soundings which were closest to the wave in distance and time were chosen for each case. The location of the sounding stations can be found in Figure 3.1. Previous studies have shown that waves generated by vertical shear instabilities tend to move with the wind speed at the level of minimum Richardson number (Atkinson, 1981). To test this hypothesis, the Richardson number was calculated and a wave speed and direction were determined from the wind speed and direction at the level of minimum Richardson number. To determine if the waves might be freely propagating, wave speeds were estimated using Equation 2.7. Wave direction was determined directly from the surface plots. The calculated wave speeds are then compared with the wave speeds determined from the PAM II data (Table 5.1) and summarized in Table 6.1.

6.1 Case 1, 4 February 1986, Sounding Data Analysis

The sounding data from FAY at 00 GMT and SSC at 00 GMT were analyzed for Case 1 (Figure 6.1). As can be seen from both plots of the Richardson number versus height, the critical value of 0.25 or less for large amplitude waves (Gedzelman and Rilling, 1978) occurs at several levels

55

Table 6.1 Gravity Wave Cases. Parameters were calculated using sounding data only. Wave speeds and directions from Table 5.1 included for comparison. Here Wspd, Wdir and sfc represent wave speed, wave direction and surface layer, respectively. Units of wave speed are in meters per second.

Case	Sounding	Forced Wave Assumption — Minimum Ri Layer, Wspd, Wdir	Freely Propagating Wave Assumption — Layers (mb)	θ (°K)	$\bar{u}$ (m s^{-1})	H (m)	Wspd Wdir	Table 5.1 Wspd Wdir
1	FAY 00 GMT	0.077 360 mb 23, 288°	(1) sfc - 730	295	5.5	2720	38 Easterly	40 Easterly
			(2) 730 - 540	307			46 Easterly	
			(2) 730 - 270	314			Easterly	
	SSC 00 GMT	0.051 900 mb 6, 230°	(1) sfc - 780	296	5.5	2199	36 Easterly	
			(2) 780 - 480	309			41 Easterly	
			(2) 780 - 250	315			Easterly	
2	GSO 12 GMT	0.11 940 mb 13, 238°	(1) sfc - 920	290	8.9	524	20 Easterly	20 - 30 Easterly
			(2) 920 - 740	298			27 Easterly	
			(2) 920 - 340	309			Easterly	
	ILM 21 GMT	0.027 770 mb 18, 281°	(1) sfc - 820	297	13.0	1776	29 Easterly	
			(2) 820 - 720	301			43 Easterly	
			(2) 820 - 330	313			Easterly	

Table 6.1, continued.

Case	Sounding	Forced Wave Assumption	Freely Propagating Wave Assumption					Table 5.1
		Minimum Ri Layer Wspd, Wdir	Layers (mb)	θ (°K)	ū (m s⁻¹)	H (m)	Wspd Wdir	Wspd Wdir
3	CHS 12 GMT	0.53 630 mb 12, 260°	(1) sfc - 790	294	8.4	2081	37 NEasterly	30 - 40 NEasterly
			(2) 790 - 600	305			44 NEasterly	
			(2) 790 - 280	313			NEasterly	
	SSC 15 GMT	0.055 710 mb 5, 243°	(1) sfc - 730	294	15.6	2686	45 NEasterly	
			(2) 730 - 600	303			58 NEasterly	
			(2) 730 - 260	315			NEasterly	
4	FAY 12 GMT	0.026 600 mb 15, 206°	(1) sfc - 760	294	2.3	2364	30 Easterly	20 - 30 Easterly
			(2) 760 - 590	304			42 Easterly	
			(2) 760 - 250	315			Easterly	
	PGV 21 GMT	0.0095 1000 mb 3, 130°	(1) sfc - 900	284	-6.0	981	11 Easterly	
			(2) 900 - 700	293			21 Easterly	
			(2) 900 - 250	308			Easterly	

Figure 6.1   Sounding Data for FAY at 00 GMT (top) and SSC at 00 GMT (bottom) on 4 February 1986.   Plotted are temperature, potential temperature, Richardson number, and wind versus height.   Dashed lines indicate levels where the Richardson number is greater than 2.0.

58

on each sounding. The minimum Richardson number on the FAY plot (Figure 6.1, top) is 0.077 at 360 mb and indicates that a forced wave should have a speed of 23 m s^{-1} with a direction out of the west-northwest. For SSC (Figure 6.1, bottom), the minimum Richardson number is 0.051 at 900 mb. Wave speed and direction should therefore be 6 m s^{-1} from the southwest. These values under the forced wave assumption do not match the wave speed and direction of 40 m s^{-1} towards the east determined from the perturbation pressure plots (Tables 5.1 and 6.1).

Under the freely propagating wave assumption, the FAY sounding (Figure 6.1, top) is analyzed. Since Equation 2.7 involves a two layer model, it is critical to determine representative layers. Layer 1 in the FAY sounding (surface to 730 mb) was capped by an inversion. The second layer (730 - 540 mb) was determined from the potential temperature versus height plot. Above 540 mb, there was a change in stability. The average potential temperature of each layer was calculated along with the average u component of the wind and height of Layer 1 (Table 6.1). Only the u component was needed since the wave moved in an easterly direction. From Equation 2.7, the wave speed was calculated as 38 m s^{-1}. If the second layer is chosen from 730 - 270 mb above which the potential temperature shows more of an increase with height, the wave speed is calculated as 46 m s^{-1}. By doing two calculations of Equation

2.7, employing different top layers, a range of possible wave speeds can be determined. For FAY this range is 38 - 46 m s^{-1}.

Looking at the SSC sounding (Figure 6.1, bottom), the first layer was from the surface to 780 mb. There was a weak inversion at 780 mb and the potential temperature indicated a change in stability. The second layer in this case extended from 780 - 480 mb. Though there appeared to be a change in stability above 480 mb, it was not as easy to determine as in the FAY sounding. Equation 2.7 parameters were determined (Table 6.1) and the wave speed was calculated as 36 m s^{-1} in an easterly direction. If the top of tne second layer is chosen as 250 mb, the wave speed is calculated to be 41 m s^{-1} (Table 6.1). This gives a range of values of 36 - 41 m s^{-1}.

From both soundings, a freely propagating wave would move in an easterly direction with a speed ranging from 36 - 46 m s^{-1}. From the PAM II data, the speed of 40 m s^{-1} falls within this range which suggests that the wave is freely propagating, rather than forced by shear instability. It is also interesting to note that the surface wave is moving faster than the wind speed at any level in either sounding.

6.2 Case 2, 5 February 1986, Sounding Data Analysis

For Case 2, the soundings for GSO at 12 GMT and ILM at

21 GMT were used (Figure 6.2). The minimum Richardson number for the GSO sounding was 0.11 at 940 mb with a wind speed out of the southwest at 13 m s^{-1}. In the case of ILM, the minimum Richardson number was 0.027 at 770 mb. Wind speed at this level was out of the west-northwest at 18 m s^{-1}. The wave speed was determined to be 20 - 30 m s^{-1} in an easterly direction from the PAM II data (Table 5.1). While the ILM speed and direction are close to the Table 5.1 values, it is still appropriate to check the values under the freely propagating assumption.

On the GSO sounding (Figure 6.2, top), Layer 1 was from the surface to 920 mb where the stability changed. Layer 2 was from 920 - 740 mb. At 740 mb, the temperature remained isothermal for about 30 mb. Parameters used in Equation 2.7 are listed in Table 6.1. The wave speed was calculated to be 20 m s^{-1} in an easterly direction. Extending the second layer to 340 mb, where the temperature started to increase with height, gave a wave speed of 27 m s^{-1}.

The potential temperature plot for ILM (Figure 6.2, bottom) determined Layer 1 to extend from the surface to 820 mb and Layer 2 from 820 mb to 720 mb. Again, as with the other soundings there was a change in stability. The wave speed was therefore calculated as 29 m s^{-1} in an easterly direction. If the second layer extends to 330 mb, the wave speed is 43 m s^{-1}.
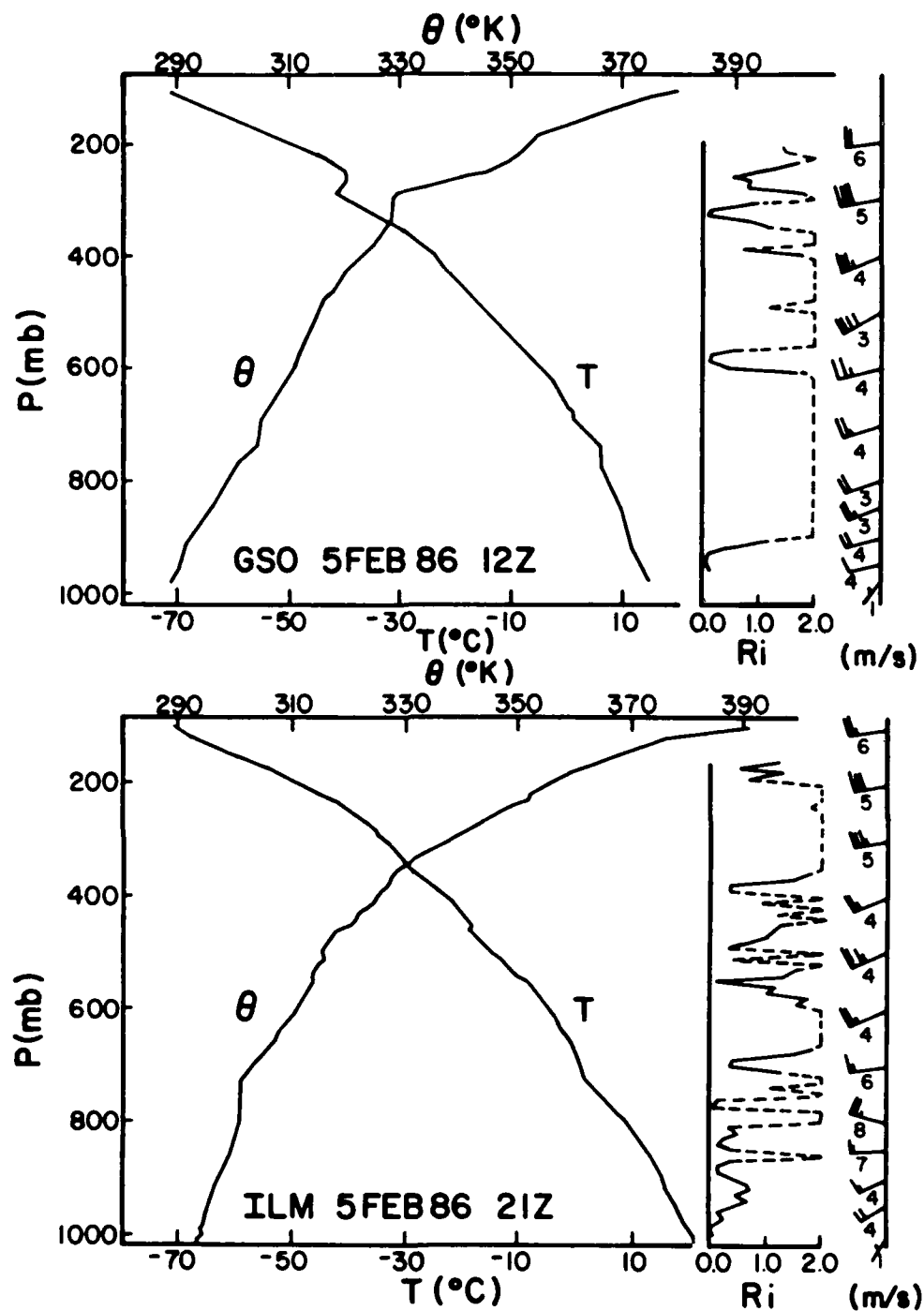
Figure 6.2   Same as Figure 6.1, except for GSO at 12 GMT
(top) and ILM at 21 GMT (bottom) on 5 February 1986.

Assuming a freely propagating wave, the wave speed can range from 20 - 43 m s^{-1} when considering both soundings (Table 6.1). This is an excellent match with the Table 5.1 values of 20 - 30 m s^{-1}. As with Case 1, it is likely that this is a freely propagating wave. However, the results from this case are not as clear as Case 1, since the observed wave speed and direction are close to the wind speed and direction near 300 mb in the GSO sounding where the Richardson number is less than 0.25. In addition, the waves in this case had a much more complicated structure than in the other cases. Thus, more than one process may have contributed to wave activity on this day.

6.3 Case 3, 6 February 1986, Sounding Data Analysis

On the CHS sounding at 12 GMT (Figure 6.3, top), all values of the Richardson number were above 0.25 with the minumum value of 0.53 at 630 mb. Wind speed at this level was 12 m s^{-1} out of the west-southwest. This was much less than the Table 5.1 value of 30 - 40 m s^{-1}. For the SSC sounding at 15 GMT, the minimum Richardson number of 0.055 at 710 mb, gave a wave speed and direction of 5 m s^{-1} out of the southwest. Again, this speed was significantly below the Table 5.1 value.

Using the freely propagating wave assumption, Layer 1 of the CHS sounding (Figure 6.3, top) was from the surface to 790 mb. This layer was capped by an inversion. The
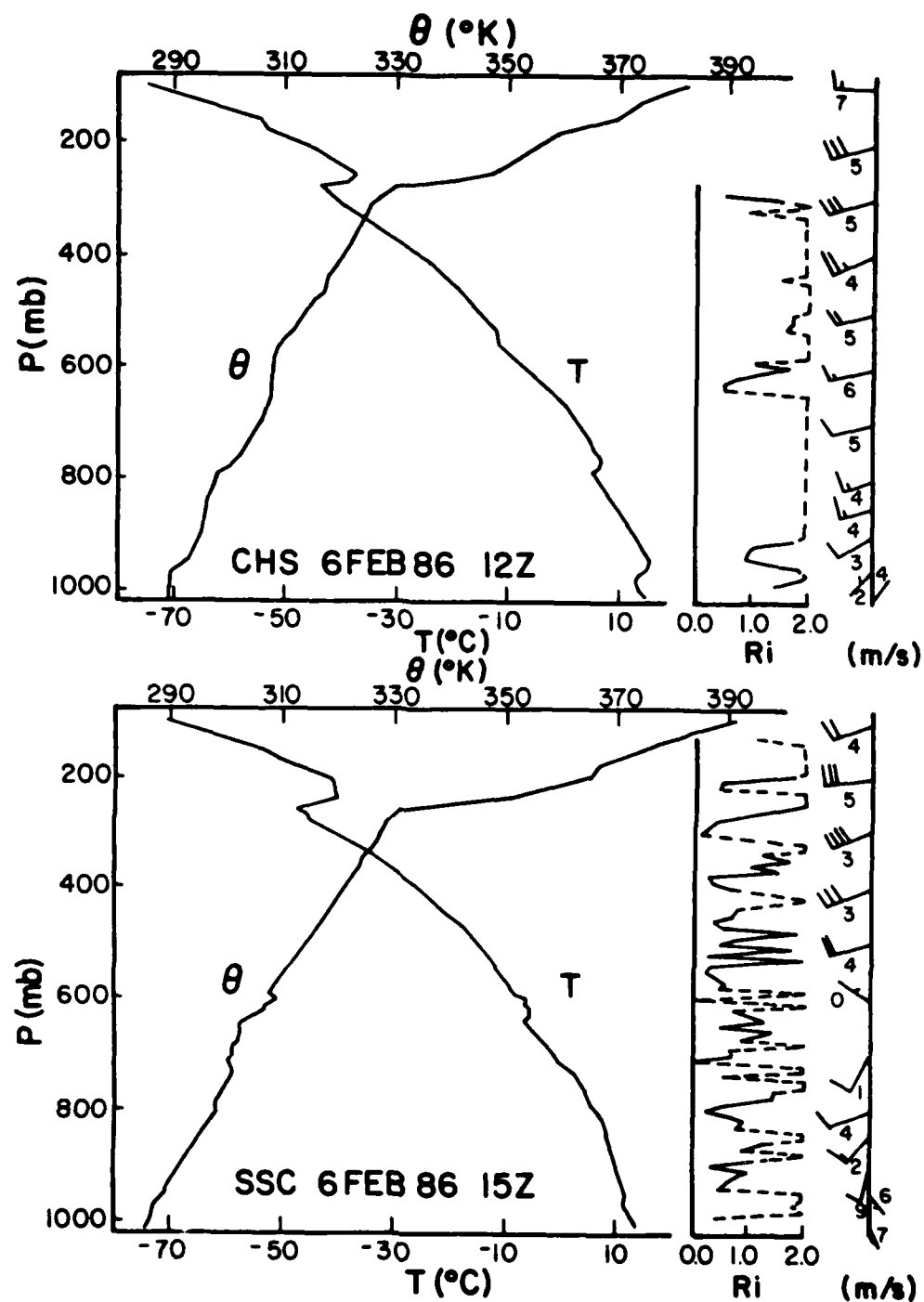
63

Figure 6.3 Same as Figure 6.1, except for CHS at 12 GMT
(top) and SSC at 15 GMT (bottom) on 6 February 1986.

64

second layer extended from 790 to 600 mb, where the stability profile changed. Since the gravity wave was moving in a northeasterly direction, a straight average of the u component of the wind in Layer 1 could not be used in Equation 2.7 as in the other cases. Instead, the component of the wind speed along the direction of wave motion was used for $\bar{u}$ in Equation 2.7. These and the other Equation 2.7 parameters are shown in Table 6.1. In the case of the CHS sounding, the wave speed was determined to be 37 m s^{-1} in a northeasterly direction. If Layer 2 is extended to 280 mb, the wave speed is calculated as 44 m s^{-1}.

Layer 1 of the SSC sounding (Figure 6.3, bottom) was from the surface to 730 mb. At this level, the potential temperature started to decrease with height. Layer 2 was capped by an inversion and extended from 730 mb to 600 mb. The component of the wind speed along the direction of the wave motion was found the same way as for the CHS sounding. The wave speed was then calculated as 45 m s^{-1}. Extending the second layer to 260 mb gave a wave speed of 58 m s^{-1}.

Considering both stations, the wave speed ranged from 37 - 58 m s^{-1}. The Table 5.1 value of 30 - 40 m s^{-1} just falls into the lower range of the Equation 2.7 value. This case can be called a freely propagating wave, though perhaps a simple two layer model may not be appropriate considering the correlation of the calculated values to the Table 5.1 range of values.

65

6.4 Case 4, 6 February 1986, Sounding Data Analysis

The FAY sounding at 18 GMT and the PGV sounding at 21 GMT were used for Case 4 (Figure 6.4). The minimum Richardson number for FAY was 0.026 at 600 mb. Wind speed was 15 m s^{-1} out of the south-southwest. For PGV, the minimum Richardson number of 0.0095 at 1000 mb yielded a wind speed of 3 m s^{-1} out of the southeast. These did not correlate at all with the Table 5.1 value of 20 - 30 m s^{-1} in an easterly direction (Table 6.1).

For the freely propagating case, Layer 1 of the FAY sounding extended from the surface to 760 mb and was capped by an inversion. Layer 2 from 760 to 590 mb was also capped by an inversion. Wave speeds were calculated to be 30 m s^{-1}. If Layer 2 was extended to 250 mb, the wave speed increased to 42 m s^{-1} (Table 6.1).

The PGV sounding had Layer 1 extending from the surface to 900 mb and Layer 2 from 900 to 700 mb. Both layers were capped by inversions. The wave speed was calculated as 11 m s^{-1}. If the second layer extended to 250 mb, the wave speed became 21 m s^{-1} (Table 6.1).

Both tne FAY and PGV soundings had the most well-defined layers of all the cases. For a freely propagating wave, the range of wave speeds were from 11 - 42 m s^{-1} (Table 6.1). These are in agreement with the Table 5.1 values of 20 - 30 m s^{-1}.
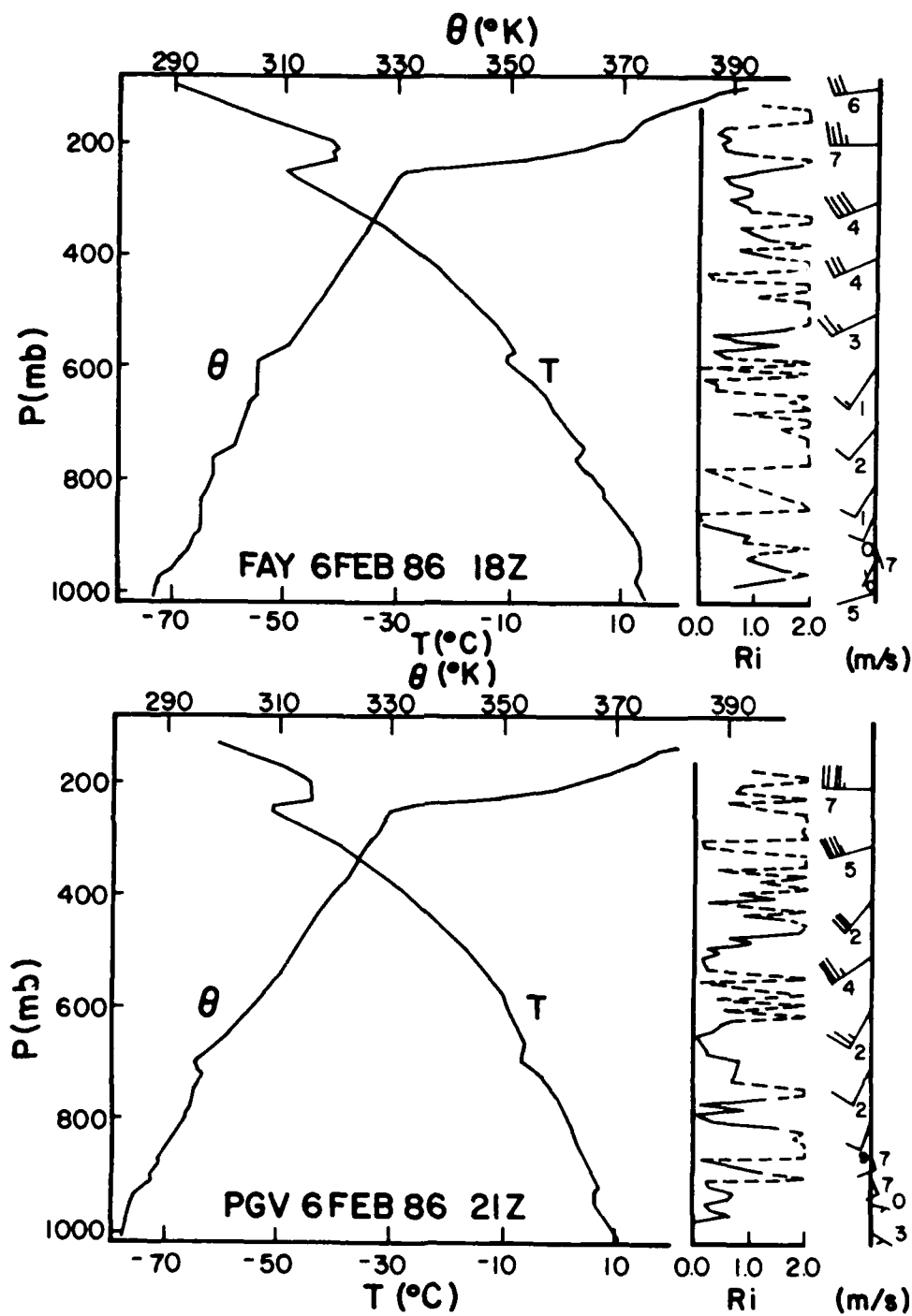
66

Figure 6.4 Same as Figure 6.1, except for FAY at 18 GMT (top) and PGV at 21 GMT (bottom) on 6 February 1986.

In the above calculations, phase speeds were determined from a simple 2-layer model. To further investigate the vertical structure of the waves, sounding data at several time periods would be needed. For Cases 1-3, data were available only at 12 hour intervals. However, data at three-hourly intervals were available for both stations of Case 4. Potential temperature was plotted versus height for the time period from 18 GMT, 6 February 1986 to 09 GMT on 7 February 1986 (Figures 6.5 and 6.6). The appropriate time of wave passage is shown on both plots. The high pressure preceding the wave is indicated by an "H" on the time axis. The "L" indicated passage of the lowest pressure as shown by the perturbation pressure plots. From the cross-sections (Figures 6.5 and 6.6), it is possible to estimate the depth of the atmosphere affected by the wave. The FAY cross-section shows no deflection of the potential temperature above 500 mb while the PGV cross-section shows a slight displacement between 300 and 500 mb during the wave passage. The maximum displacement occurs between 800-600 mb in both cross-sections. This suggests that this wave is a middle-to-lower troposphere perturbation. This provides further evidence that this wave is freely propagating rather than resulting from shear instability associated with the jet stream winds at upper levels.
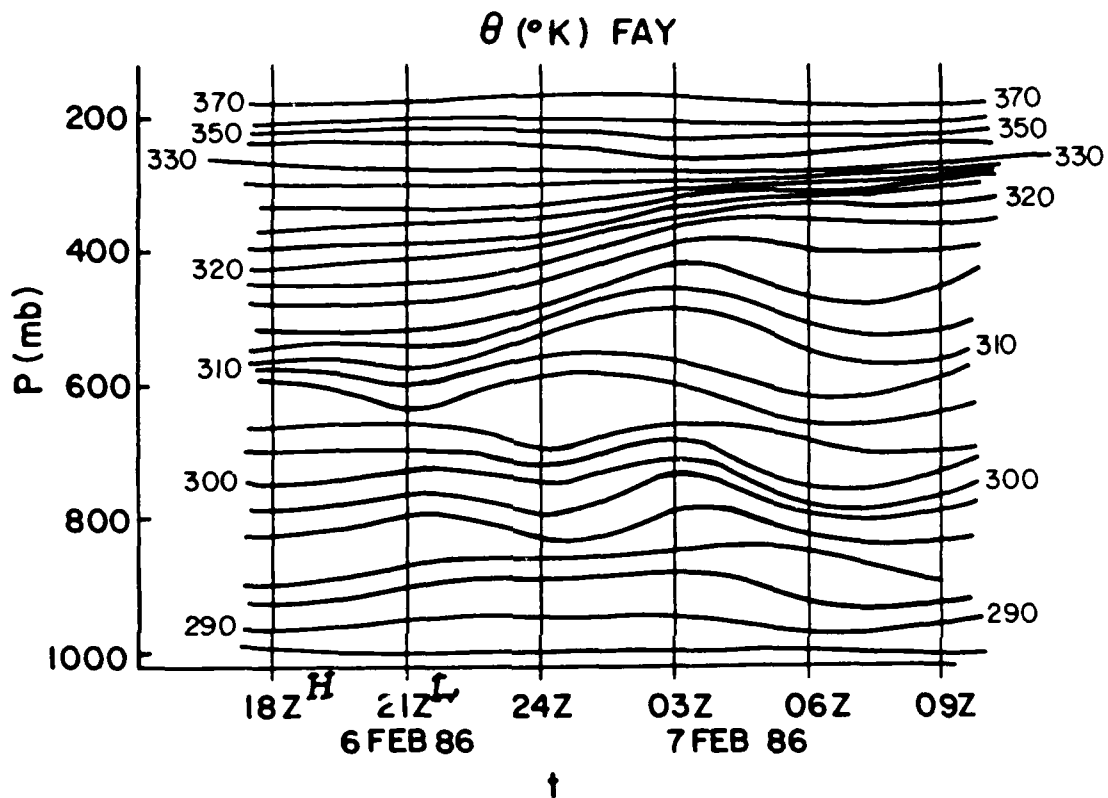
68

Figure 6.5 Potential temperature versus height at 3-hour intervals from 18 GMT, 6 February 1986 to 09 GMT, 7 February 1986 for Fayetteville, NC (FAY).
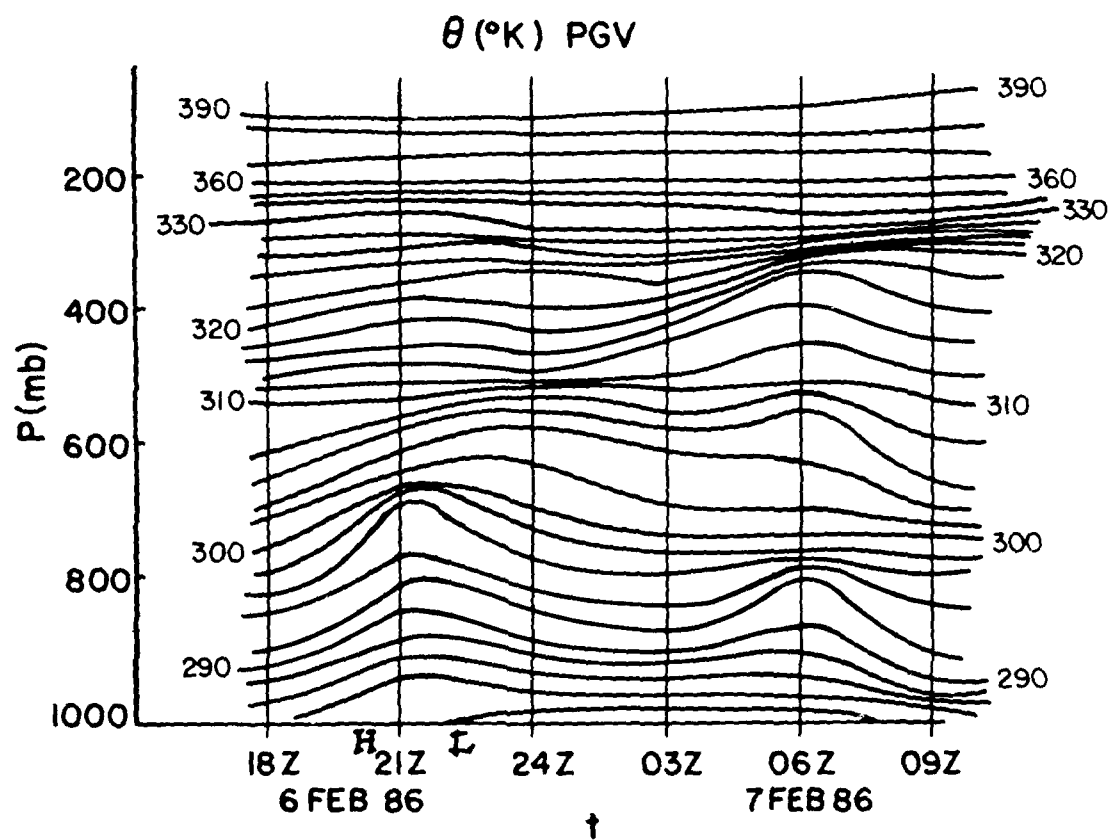
64

Figure 6.6   Same as Figure 6.5, except for Greenville, NC (PGV).

70

7. SUMMARY AND CONCLUSIONS

During the Genesis of Atlantic Lows Experiment, a tnree-day period from 4 to 6 February 1986 was analyzed to check for the occurrence of gravity waves. Several mesoscale disturbances resembling gravity waves passed through the data network during that time.

Tne diurnal and semi-diurnal trends were removed from the high resolution pressure, temperature, and wind fields, using a high-pass spectral filter. Higher frequencies with periods of 8 hours or less were therefore isolated. An objective analysis scheme was used to interpolate the data onto an evenly spaced grid. A spatial filter was also applied to remove wavelengths less than twice the original station spacing. Using the filtered wind field, the horizontal divergence was calculated.

Four gravity wave cases were identified from the perturbation pressure and horizontal divergence fields. Phase speeds ranged from 20 - 40 m s^{-1} with wavelengths from 200 - 400 km, and amplitudes of 0.25 - 2.0 mb. Hourly rainfall was plotted on the data grid and analyzed for possible correlation with each gravity wave case. Only for the last case on 6 February did the precipitation follow the movement of tne wave. This was also the most well-defined of all the four cases.

Furtner analysis was done using sounding data.

71

Assuming a simple two-layer model, it appeared that Cases 1, 3 and 4 were freely propagating versus forced by an upper level disturbance. For Case 2, several different processes may have contributed to wave activity.

If the waves were freely propagating, this implies that their source region was outside of the analysis region of the PAM stations. Cases 1, 2 and 4 were oriented from north to south and moved from the west to the east. This orientation of the waves was perpendicular to the warm front located in the northern data field, thus making it unlikely that they were caused by that front. The orientation of the waves in Cases 1, 2 and 4 suggests that the Appalachian Mountains may have played a role in their formation. Though the waves were analyzed as freely propagating, the cold front and surface cyclone to the west of the mountains may also be linked to the wave formation. Case 3 was oriented from the west to the east and moved in a northeasterly direction suggesting a different source mechanism than the other cases. Case 3 was analyzed to be a freely propagating wave though there was a possibility that it might have been forced. An upper level disturbance to the south of the wave might have been the forcing mechanism. There also was thunderstorm activity in northern Florida occurring at the time.

Although three of the four cases did not have precipitation patterns moving with them, there were

convergence and divergence patterns associated with the waves, especially for Cases 2 and 4. Gravity waves may then be a triggering mechanism for precipitation in regions far from the source regions of the waves.

Further analysis of gravity wave phenomenon should be done employing more cases than presented here. Also, by using a tnree-or-four-layer model, where appropriate, a more accurate determination can be made of wave speeds and directions. A two-layer model can be used where there are well-defined layers as in Case 4.

8. LIST OF REFERENCES

Atkinson, B.W., 1981: Meso-scale Atmospheric Circulations. Academic Press, pp. 283-309.

Bannon, P.R., 1979: On the Dynamics of the East African Jet. I: Simulation of mean conditions for July. J. Atmos. Sci., 36, 2139-2152.

Barnes, S.L., 1964: A Technique for Maximizing Details in Numerical Weather Map Analysis. J. Appl. Meteor., 3, 396-409.

_____, 1973: Mesoscale objective map analysis using weighted time-series observations. NOAA Techical Memorandum ERL NSSL-62, Norman, OK, 60 pp.

Bloomfield, P., 1976: Fourier Analysis of Time Series: An Introduction. John Wiley & Sons, 258 pp.

Bosart, L.F., 1973: Detailed Analysis of Precipitation Patterns Associated with Mesoscale Features Accompanying United States East Coast Cyclogenesis. Mon. Wea. Rev., 101, 1-12.

_____, and J.P. Cussen, 1973: Gravity Wave Phenomena Accompanying East Coast Cyclogenesis. Mon. Wea. Rev., 101, 446-454.

Cunning, J.B., 1974: Tne Analysis of Surface Pressure Perturbations within the Mesoscale Range. J. Appl. Meteor., 13, 325-330.

Donn, W.L., S.D. Gedzelman, and N.K. Balachandran, 1973: Atmospheric Gravity Waves and the Energy of the Jet Stream. Bull. Amer. Meteor. Soc., 54, 633-636.

Gedzelman, S.D., 1983: Short-Period Atmospheric Gravity Waves: A Study of their Statistical Properties and Source Mechanisms. Mon. Wea. Rev., 111, 1293-1299.

_____, and R.A. Rilling, 1978: Short-Period Atmospheric Gravity Waves: A Study of their Dynamic and Synoptic Features. Mon. Wea. Rev., 106, 196-210.

Gossard, E., and W. Munk, 1954: On Gravity Waves in the Atmosphere, J. of Meteor., 11, 259-269.

Herron, T.J., and I. Tolstoy, 1969: Tracking Jet Stream Winds from Ground Level Pressure Signals. J. Atmos. Sci., 26, 266-269.

      , and D.W. Kraft, 1969: Atmospheric Pressure Background Fluctuations in the Mesoscale Range. J. Geophys. Res., 6, 1321-1329.

Hobbs, P.V., et. al., 1985: Genesis of Atlantic Lows Experiment, GALE Experiment Design. GALE Project Office, 199 pp.

Holton, J.R., 1979: An Introduction to Dynamic Meteorology. Academic Press, 391 pp.

Hooke, W.H., and K.R. Hardy, 1975: Further Study of the Atmospheric Gravity Waves over the Eastern Seaboard of 18 March 1969. J. Appl. Meteor., 14, 31-38.

Mastrantonio, G., F. Einaudi, and D. Fua, 1976: Generation of Gravity Waves by Jet Streams in the Atmosphere. J. Atmos. Sci., 33, 1730-1738.

Shapiro, R., 1975: Linear Filtering. Math. Comp., 29, 1094-1097.

Tolstoy, I., and T.J. Herron, 1969: A Model for Atmospheric Pressure Fluctuations in the Mesoscale Range. J. Atmos. Sci., 26, 270-273.

END

Feb.

1988

DTIC